SCEP1 and SCEP2 are two new components of the synaptonemal complex central element

Nathalie Vrielynck[1#], Marion Peuch[1#], Stéphanie Durand[2], Qichao Lian[2], Aurélie Chambon[1], Aurélie Hurel[1], Julie Guérin[1], Raphael Guérois[3], Raphael Mercier[2], Mathilde Grelon[1, $], Christine Mézard[1,4,$]

1 : Université Paris-Saclay, INRAE, AgroParisTech, Institut Jean-Pierre Bourgin (IJPB), 78000, Versailles, France.

2 : Department of Chromosome Biology, Max Planck Institute for Plant Breeding Research, Carl-von-Linné-Weg 10, Cologne, Germany

3 : Université Paris-Saclay, CEA, CNRS, Institute for Integrative Biology of the Cell (I2BC), 91198, Gif-sur-Yvette, France.

4 : Université Paris-Saclay, INRAE, AgroParisTech, CNRS, Institut Jean-Pierre Bourgin (IJPB), 78000, Versailles, France.

# the two authors have contributed equally to this work

$ corresponding authors: Christine.mezard@inrae.fr; Mathilde.grelon@inrae.fr

Abstract

The synaptonemal complex (SC) is a proteinaceous structure that forms between homologous chromosomes during meiosis prophase. The SC is widely conserved across species, but its structure and roles during meiotic recombination are still debated. While the SC central region is made up of transverse filaments (TF) and central element proteins (CE) in mammals and fungi, few CE proteins have been identified in other species. Here we report the identification of two coiled-coil proteins, SCEP1 and SCEP2, that form a complex and localize at the center of the *Arabidopsis thaliana* SC. In *scep1* and *scep2* mutants, chromosomes are aligned but not synapsed (the ZYP1 TF protein is not loaded), crossovers (COs) are increased compared to the wild-type, interference is lost, and heterochiasmy is strongly reduced. We therefore report the identification of the first plant SC central elements, and homologs of these are found in all major angiosperm clades.

Main text

In meiosis, haploid cells are formed by executing two successive rounds of cell divisions occurring after one step of DNA replication. In many species, the crossovers (COs), which are an exchange of genetic material produced by recombination between homologous chromosomes, are essential for the correct segregation of chromosomes during the first meiotic division. Concomitant with the molecular events forming the COs during prophase of the first meiotic division, each pair of homologous chromosomes becomes tightly synapsed to each other along their entire length by a proteinaceous structure known as the synaptonemal complex (SC)[1] **.** Cytological observations performed in many species have described the SC as a zipper-like tripartite structure with two rods forming the lateral elements (LE), one at the base of each pair of sister chromatids, and a multilayered central region[2]. The SC central region is composed of transverse filaments (TF) and, in many species, central element (CE) proteins. TFs are formed by dimers of long coiled-coil proteins (ZYP1A and ZYP1B in *Arabidopsis thaliana*[3–5], Zip1 in *Saccharomyces cerevisiae*[6]*,* SCYP1 in mice[7], SYP-1, SYP-5, and SYP6 in *Caenorhabditis elegans*[8,9,10] and, C(3)G in *Drosophila*[11]) with their N-terminal globular domains arranged head-to-head in the center of the SC and their C-terminus at the LE[12]. Thirteen different CE proteins have been identified: five in mice (SYCE1, SYCE2, SYCE3, TEX12, and SIX6OS1)[13–16], three in *C. elegans* (SYP-2, SYP-3, and SYP-4)[17–19], two in *S. cerevisiae* (Ecm11 and Gmc2)[20], and two in *Drosophila* (CONA and Corolla)[21,22]. No significant sequence similarity between CE proteins across species has been identified, but they often display either a long alpha helix or a coiled-coiled structure[23]. CE proteins have been shown to promote the polymerization, stabilization, and/or reorganization of TFs[24]. The absence of CE proteins has different consequences, depending on the model species. In mice, *C. elegans,* or Drosophila, loss of any CE protein leads to severe meiotic defects and sterility, synapsis is impaired and crossovers are not formed[13-19,21,22]. In *S. cerevisiae,* in the absence of Ecm11 or Gmc2, sporulation is delayed, spore viability is only slightly reduced, the TF protein Zip1 exhibits a dotty pattern but COs are formed and found to be increased on certain chromosomes [20].

CE proteins associate in sub-complexes through their alpha helix or coiled-coil regions, and the complexes self-assemble to form higher-order structures with different roles within the SC. For example, in mice, the SYCE3 protein self-assembles and remodels TF organization[25]. SYCE3 also interacts with the two CE subcomplexes SIX60S1-SYCE1 and TEX12-SYCE2, providing a means for their recruitment on the SC[25]. Biochemical and biophysical analyses

suggest that each high-affinity sub-complex formed by SYCE3-SYCP1, TEX12-SYCE2, and SYCE1-SIX6OS1 assembles into higher structures (self or hetero-assembled lattices and/or fibers) and that the three sub-complexes transiently interact by low-affinity connections that are dynamic during SC formation [25]. The mammalian TEX12-SYCE2 complex exhibits structural and functional similarities to the yeast Ecm11-Gmc2 protein complex[26]. Both Ecm11 and TEX12 interact with the ZMM protein Zip4 in yeast and the mouse Zip4 homolog TEX11 which belong to the ZMM (Zip1-4, Msh4-5, Mer3, Spo16) group of protein which control the formation of most COs. Moreover, AlphaFold2 predicts that Ecm1 and Gmc2 form a tetramer[26] very similar to the crystal structure obtained for the TEX12-SYCE2 tetramer[27]. In *C. elegans*, the localization of each SYP protein is dependent on the presence of all the other SYPs confirming that they all participate in a common structure[8,17–19]. SYP-3 and SYP-4 form a complex with the SYP-3 C-terminus located close to the LE and SYP-4 N-terminus in the center of the SC. The small SYP-2 protein interacts with the SYP-1 N-terminus and localizes at the SC center[28]. The two Drosophila CE proteins CONA and Corolla also interact with each other, with CONA localizing close to the N-terminus of the C(3)G TF[22,29]. The localizations of CONA, Corolla, and C(3)G depend on each other. Considering the crucial role of CE proteins in the structure and functions of the SC in various species, it is intriguing that no CE proteins have been identified in plants, and the question remains as to whether CE proteins exist outside metazoa and fungi.

In order to identify new meiotic players in *Arabidopsis thaliana,* we set up a screen based on transcriptomic data. Here, we describe the identification of two new small coiled-coil proteins, SCEP1 and SCEP2. Orthologs of these two proteins could be detected in all major Angiosperm clades as well as in more distant species such as ferns (within the Tracheophytes clade) but not in other species such as mosses or algae. SCEP1 and SCEP2 interact with each other, colocalize with ZYP1 in the central region of the SC, and are mutually interdependent for their loading on the SC. When mutated, TFs are not formed, synapsis does not occur, and COs are increased. Altogether, these data suggest that SCEP1 and SCEP2 belong to the central element of the SC and participate in the control of CO formation.

RESULTS

Identification of SCEP1 and SCEP2

From the analysis of the transcriptomic data published in[30], we noticed that 23 out of the 27 genes known to have a specific role in *Arabidopsis thaliana* meiosis (*ASY1, ASY3, ASY4, DFO, DMC1, DUET, HEI10, JASON; MER3, MSH4, MSH5, MTOPVIB, OSD1, PCH2, PHS1, PRD1, PRD2, PRD3, PTD, REC8, SCHOC1, SDS, SPO11-1, SPO11-2, SWI1, ZYP1A, ZYP1B, ZIP4*) had an expression peak at a stage where flower buds have a size of about 0.5 mm (Fig. 1A, Supplementary Table1). This size marks the stage at which male meiosis takes place within the flower buds[31]. We analyzed the expression profile of the full set of *A. thaliana* genes in flowers and selected 80 genes that presented an expression profile similar to that of known meiotic genes (Material and Methods). Among them, we selected the gene *AT1G33500*, hereafter called *SCEP1*, for further characterization.

Using CRISPR-Cas9 with three gRNAs targeting three different sites in *SCEP1* (Fig. 1, Extended Data Figure 1), six independent mutations were identified in the Columbia accession with various insertions/deletions leading to a frameshift at several positions: after the first 20 amino-acids (aa) for *scep1-1* and *scep1-2*, after the first 55 aa for *scep1-3* and after the first 114 aa for *scep1-4*, *scep1-5*. *scep1-6* had a deletion of 96 aa between aa 20 and 116. We also obtained a mutation in the Landsberg *erecta* accession (*scep1-7*) with a premature stop codon at the same position as in *scep1*-1 (Extended Data Figure. 1).

We explored chromosome behavior during male meiosis in the *scep1* mutant series. In chromosome spreads stained with DAPI, 10 to 25% of the cells at metaphase I exhibited one or two pairs of univalents instead of the five pairs of bivalents observed in 100% of the wild-type meiocytes (Fig. 1B-C). As an expected consequence of this defect in bivalent formation, unequal segregation of chromosomes was observed at anaphase I-metaphase II-anaphase II with a 6:4 chromosome distribution in 7 to 20% of the cells (Fig. 1B; Supplementary Figure 1). Thus, in the absence of SCEP1, there is a failure to form at least one CO per bivalent. At earlier prophase stages, *scep1* leptotenes were not different from wild-type leptotenes. At the pachytene stage, in wild-type meiosis, homologous chromosomes are fully synapsed, and appear as fluffy structures in which the two homologous chromosomes are paired and hardly distinguishable from each other. However, in *scep1* mutant cells, we observed that large chromosome regions were aligned and remained distinguishable one from the other (unsynapsed) (Supplementary Figure 1), and typical pachytene stages were never observed (n=50).

The transcriptomic data from[30] predicted two isoforms of SCEP1 differing in the 3' terminal part of the proteins. After sequencing the 3' ends of cDNAs, only the short form corresponding to a 254 aa protein was found (see Material and Methods and Extended Data Figure. 1). SCEP1's structure was analyzed using AlphaFold2[32]. Five separate structure predictions were performed, and showed high levels of similarity with each other. It was predicted with a high probability (76% of residues have pLDDT above 85) to be a small coiled-coil protein with two long alpha-helices; the short region between the two alpha-helices around the middle of the protein (aa 135 to 144) had a low pLDDT value indicating that the protein might not fold as depicted in Fig. 1E.

Using the ColabFold notebook[33], we explored the predicted structure of proteins with a meiotic-like profile of expression (Fig. 1A). *AT3G28370*, referred to as SCEP2, was predicted to have a very similar structure to SCEP1: a small coiled-coil protein with two alpha-helices separated by a small unstructured region (residues 136-153). As for SCEP1, the predicted C-terminus part of SCEP2 was uncertain. After sequencing the cDNAs, two isoforms were found that differ in the last 45 amino acids with a long (262 aa) and a short (227 aa) protein. This variable C-terminus is poorly predicted by AlphaFold2 (Fig. 1E, Extended Data Figure. 1D-F). We examined the behavior of the chromosomes in the line N663933 (*scep2-1*), where the T-DNA was inserted in the second exon of the gene (Fig. 1D, Extended Data Figure. 1D, F). The meiotic defect observed was similar to the one observed in the *scep1* alleles: around 10% of metaphase I had a default in bivalent formation with one pair of univalents (6/54), 5% of metaphase II – anaphase II had a 6:4 chromosome distribution (3/83) and no true synapsis in prophase I was observed (Fig1. B-C; Supplementary Figure 1).

We measured the fertility of *scep1-1* and *scep2-1* mutant plants by counting the number of seeds per silique. We found that the fertility was slightly reduced compared to the wild-type plants with 58.9 and 57.2 seeds per silique in *scep1-1* ($p=4x10^{-4}$) and *scep2-1* ($p<10^{-5}$) respectively compared to 63.3 in wild type (Fig. 1F, Supplementary Table 8).

In conclusion, we identified two small coiled-coil proteins, SCEP1 (*AT1G33500*) and SCEP2 (*AT3G28370*), which are required for efficient formation of chromosome bivalents at metaphase I and for full fertility.

SCEP1 and SCEP2 are required to form transverse filaments

DAPI staining of chromosomes suggested that synapsis was defective in *scep1* and *scep2* mutants. We wondered whether the ZYP1 proteins that form the TF structure of the SC were normally loaded in *scep1* and *scep2* mutants. We performed immunolocalization of the axis protein ASY1 together with ZYP1. In wild-type pachytene cells, the ZYP1 signal forms a continuous line along the synapsed chromosomes, while the ASY1 labelling is faint due to its partial removal from the chromosome axes[31,34] (Fig. 2A). In *scep1-1* and *scep2-1*, however, there was no ZYP1 signal and the ASY1 labeling did not weaken in zygotene-like or pachytene-like cells (Fig. 2A). Moreover, the two axes appear as two parallel lines instead of a weak single line as in wild type, suggesting that chromosome pairing occurs but not synapsis.

Using ASY1 and REC8 immunolocalization and stimulated emission depletion (STED) microscopy on wild-type pachytene cells, we were able to visualize the two parallel LE axes along the synapsed chromosomes, at a distance of 175±23 nm (Fig. 2B-C). In *scep1-1* and *scep2-1*, the two axes decorated by REC8 and ASY1 were also aligned but at a mean distance of 285±68 nm which is 1.6-fold the distance observed in the wild-type (Fig. 2B-C). In addition, the distance between the two axes has a higher variability in *scep1* and *scep2* mutants than in the wild type (Fig. 2C). Thus, in the absence of SCEP1 and SCEP2, pairing occurs, but ZYP1 proteins are not loaded on the SC, and synapsis does not take place.

SCEP1 and SCEP2 localize in the middle region of the SC

We raised antibodies against SCEP1 and SCEP2 and analyzed their localization on chromosome spreads during male meiosis together with ASY1 and/or ZYP1. In *scep1-1* cells, no signal was observed with the SCEP1 antibody in male meiocytes. Likewise, no signal was seen with the SCEP2 antibody in *scep2-1* meiocytes either (Extended Data Figure. 2). In wild-type cells, both the SCEP1 and the SCEP2 signals were first seen at zygotene stage on synapsed chromosomal regions identified by faint ASY1 labelling and bright ZYP1 signals with which they perfectly colocalize (Fig. 3). We did not observe one of the three proteins SCEP1, SCEP2 or ZYP1 being loaded before the others. At the pachytene stage, SCEP1 and SCEP2 decorate the full length of synapsed chromosomes and perfectly colocalize with the ZYP1 signal (Fig3. B-D). Using STED microscopy, we compared the localization of SCEP1 and SCEP2 to ZYP1 and REC8. SCEP2 formed a single line lying between the two parallel lines formed by REC8 (Fig. 4A). In *Arabidopsis*, as in other species, the TF proteins were shown to have their globular carboxyl termini associated with the lateral axes of the homologs and the N termini overlapping in the

central region of the SC[4,5]. The accurate localization of SCEP2 was further investigated using an antibody raised against the very C-terminus part of ZYP1 that labels the most external part of the TF (See Material and Method). We observed that SCEP2 is localized between the two ZYP1 C-terminus signals (Fig. 4B), showing its central localization on the central region of the SC. When REC8 and SCEP1 were co-immunolocalized, SCEP1 localized between the two REC8 lines (Fig. 4C). In some regions the SCEP1 signal was compatible with the formation of a double line between the two REC8 axes whereas in other places a single line could be seen in the center of the SC (Fig. 4C). We also observed that when SCEP1 and SCEP2 co-immunolocalized, SCEP2 broadly colocalized with the SCEP1 signal that closely surrounds some portions of the SCEP2 signal (Fig. 4D). When two SCEP1 lines were detected, they were distant by 95 ± 19 nm, and thus within the two ZYP1 C-terminus lines distant by 170 nm (Fig. 4E). Therefore, we can conclude that SCEP1 and SCEP2 both localize in the middle of the central region of the SC.

SCEP1, SCEP2 and ZYP1s are needed to form the SC

As reported above, ZYP1 proteins were not detected between the two LE in the *scep1-1* and *scep2-1* mutants (Fig. 2A). We wondered if the opposite was true. We immunolocalized SCEP1 in *scep2-1* meiocytes and in the null *zyp1-1* line[4] and did not obtain any signal (Fig. 5A,n=11 and n=21 respectively). Reciprocally, SCEP2 was also undetectable in both *scep1-1* and *zyp1-1* mutants (Fig. 5B, n=25 and n=11 respectively).

The meiotic defects observed in each single mutant *scep1-1*, *scep2-1* and *zyp1-1* are indistinguishable (see above). We then analyzed the double mutants *scep1-1 zyp1-1*, *scep2-1 zyp1-1* and *scep1-1 scep2-1* and found that they had the same phenotype as each single mutant in terms of bivalent formation defects, unequal segregation at metaphase 2 (Fig. 1C), and absence of synapsis (Supplementary Figure 2). Therefore, these three genes act via the same pathway and the formation of a full SC depends on each of the three proteins SCEP1, SCEP2 and ZYP1.

SCEP1 and SCEP2 form a complex

As the phenotypes of *scep1*, *scep2,* and *zyp1* mutants were identical and their loading on the SC was interdependent, we wondered whether these proteins could interact together. AlphaFold2 predicted that SCEP1 and SCEP2 could form a parallel heterodimer with high ipTM scores and low PAE values for the two N-alpha helices interacting with each other and the two

C-alpha helices also interacting with each other (Fig. 6A). It should be noted that prediction of the disordered structure between the two alpha helices of each protein is still poorly predicted when the two proteins are in a complex. Yeast two-hybrid assays confirmed that SCEP1 and SCEP2 interact with each other even on the most stringent culture media (Fig. 6B and Supplementary Table2). Using SCEP1 and SCEP2 truncations in the yeast two-hybrid analyses, we confirmed the predicted interaction between the SCEP1 and SCEP2 C-terminus helices. However, the N-terminal helix of SCEP1 interacted only weakly with the N-alpha helix of SCEP2. AlphaFold2 also predicted with good confidence the formation of parallel SCEP1 and SCEP2 homodimers (Fig. 6A), and strong interactions were detected by yeast two-hybrid assays with full length and truncated proteins (Fig. 6B and Supplementary Table2). We also tested if SCEP1 and SCEP2 interacted with ZYP1. None of the SCEP1 and SCEP2 constructs, either full length or truncated, were able to interact with ZYP1 full length, N-terminus or C-terminus (Fig6B). AlphaFold2 did not predict an interface between SCEP1, SCEP2, and ZYP1 either. In yeast and mice, Ecm11 and TEX12 interact with the C terminal part of Zip4 and TEX11 (the mice ortholog of the budding yest Zip4) respectively[26]. We did not detect any interaction between ZIP4 C-terminus and SCEP1 or SCEP2 (Fig. 6B), both through yeast-two hybrid assays and AlphaFold2 predictions.

SCEP1 and SCEP2 limit class I COs, impose interference and heterochiasmy

We immunolocalized the MLH1 protein that specifically marks a subset of COs called class I COs in *scep1-1*, *scep2-1*, and *scep1-1 scep2-1* male meiocytes. We observed a 50% increase in MLH1 foci in the two single mutants *scep1-1* and *scep2-1* and in the double mutant *scep1-1 scep2-1* (Fig. 7A), similar to the CO increase reported for the *zyp1* mutants[4]. To verify whether this increase in MLH1 foci reflected an increase in COs, we generated genetic maps for male and female meiosis. We crossed heterozygous *scep1-1* in the Columbia (Col-0) background with heterozygous *scep1*-7 in the Landsberg (*Ler*) background to produce Col x *Ler* F1 hybrids with two mutant *scep1* alleles. In terms of bivalent formation, the F1 Col x *Ler scep1-1/scep1-7* was indistinguishable from a Col-0 *scep1* mutant (Fig. 1C-D). These mutant F1s were used as male or female when backcrossing with the wild-type parent Col-0. The progeny was sequenced to obtain the number of COs and their localization. In progeny derived from *scep1-1/scep1-7* male meiosis, the average number of COs was 7.53 ± 2.3 (mean ± sd) per gamete (n=143) confirming a large increase (+40%, Mann-Whitney test, two sides $p< 2.2\ 10^{-16}$)

compared to wild-type (5.4 ± 1.9)[35] (Fig. 7B). This CO increase seen in *scep1-1/scep1-7* is similar to the increase in MLH1 foci observed in male meiocytes (Fig. 7A). An even higher increase was found in female meiosis with 6.6 ± 2.7 (n=142) COs in *scep1-1/scep1-7*, which was largely above the wild-type level (2.79 ± 1.3, $p < 2.2x10^{-16}$) (Fig. 7B). In wild type, the frequency of CO counts was higher in male than female (+90%, $p < 2.2x10^{-16}$), a phenomenon called heterochiasmy. In *scep1-1/scep1-7*, the heterochiasmy was largely reduced but still significant (+14%, $p = 8.4x10^{-5}$).

In *scep1*, an increase in CO frequencies was observed along chromosome arms, and particularly toward the chromosome ends (Fig. 7E). By contrast, in the pericentromeric regions fewer COs were observed in *scep1* than in wild type. Both effects are clearer in female than male as the global CO increase is larger in female meiosis than in male meiosis (+136% vs +40% (Fig. 7B)). Thus, SCEP1 influences the CO landscape along the chromosomes both in male and female meiosis.

Interference is defined by the observation that COs do not occur close to each other on the same chromosome and are more evenly and distantly spaced than expected if distributed independently[36,37]. The observed distributions of the distances between two COs were very different in the *scep1* mutant compared to the ones observed in wild type meiosis for both sexes. In wild-type meiosis, due to interference, COs are more widely spaced apart (Fig. 7C) compared to the expected distribution without interference (grey distribution in Fig. 7C). By contrast, in *scep1*, both in male and female meiosis, double COs tend to occur at shorter distances and were not significantly different from the expected distribution in the absence of interference. This absence of interference in the *scep1* mutant was confirmed by plotting the coefficient of coincidence (CoC) along the chromosomes. The CoC represents the frequency of COs occurring in two different intervals of the same chromosome in a single meiosis divided by the product of the frequencies of COs in each interval (which is the expected frequency of double COs if they were independent). When CoC equals one, it means that a CO formed in one interval does not interfere with the occurrence of a CO in the second interval. By contrast, the closer to zero the CoC is, the more the concomitant occurrence of two COs in two intervals is rare. In wild type, the CoC was close to 0 when the distance between the pairs of considered intervals was shorter than 5 Megabases (Mb) and 8 Mb in male and female meiosis respectively, reflecting that interference prevents the formation of close double-CO (Fig. 7D,[4]). The CoC reached 1 at ~10 Mb in male and ~15 Mb in female wild

type meiosis showing that interference faded at these distances. In the *scep1-1/scep1-7* mutant, the CoC curve was close to 1 regardless of the distance between intervals, in both male and female meiosis (Fig. 7D), suggesting that there is no interference in the absence of SCEP1.

Results obtained for *scep1* were compared to those obtained in the *zyp1* mutant[4]. The number of COs was not significantly different between *scep1* and *zyp1*, for both female and male meiosis (p=0.08 and 0.05, respectively) (Fig. 7B), interference was abolished in both contexts (Fig. 7C-D,[4]), and the CO distributions were comparable (Fig. 7E, Extended Data Figure 3). However, heterochiasmy was strongly reduced but not abolished in *scep1*, with male gametes having only 14% more crossovers than female gametes (p<0.001), compared to +94% in wild type (p<0.0001), and absence of heterochiamsy in *zyp1* (p=0.32).

SCEP1 and SCEP2 homologs are found in Angiosperms

Through a PSI-BLAST approach, the presence of SCEP1 and SCEP2 homologs based on sequence identity in a representative set of plant species was inferred. Homologs for both SCEP1 and SCEP2 were found in all major angiosperm clades, including the basal angiosperm *Amborella trichopoda* (Fig. 8). Outside Angiosperms, homologs were also found in *Selaginella moellendorffii.* Reciprocal PSI-BLAST best hit searches starting from the homologs found in *Selaginella* and from the chosen angiosperms *Amborella*, *Jatropha curcas*, *Solanum lycopersicum* and *Gossypium raimondii* were performed and confirmed that these are indeed SCEP1 and SCEP2 homologs since the only homologs found in *Arabidopsis* are SCEP1 and SCEP2 respectively. Moreover, the SCEP1 and SCEP2 homologs found in the above species were predicted to interact with significant confidence levels using AlphaFold2 (ipTM scores of 0.7, 0.6, 0.5, 0.6, and 0.5 respectively, see Extended Data Figure 4). Beyond flowering plants (Angiosperms) and lycophytes (*Selaginella moellendorffii*), the sequence search was not sensitive enough to find SCEP1 and SCEP2 homologs. As previously reported [38], ZYP1 homologs were found in all angiosperms as well as in the gymnosperm *Taxus chinensis* and the bryophyte *Marchantia polymorpha*.

Discussion

In contrast to animals and fungi, no protein specific to the central element of the synaptonemal complex was known in plants. Here, we described the identification of two new meiotic proteins SCEP1 and SCEP2. These proteins are small coiled-coil proteins. They both localize in the middle of the central region of the SC, together with the N terminal part of ZYP1. The localizations of the three proteins, SCEP1, SCEP2, and ZYP1, depend on each other. Moreover, the meiotic defects observed in the *scep1* and *scep2* mutants phenocopy the ones reported in the *zyp1* mutant[4,5]: pairing of homologous chromosomes but no synapsis, CO increase but loss of interference as well as reduction of heterochiasmy. In addition, COs are redistributed in a similar way to *zyp1* with an increase of distal COs and a reduction of pericentromeric COs. All these data led us to conclude that SCEP1 and SCEP2 are the first CE proteins identified and characterized in plants.

Described CE proteins are known to associate and form subcomplexes: Ecm11 with Gmc2[20], Cona with COROLLA[21,29], SYP-3 with SYP-4[28], SYCE1 with SIX6OS1[16], SYCE2 with TEX12[15]. We demonstrated that SCEP1 and SCEP2 interact with each other in yeast two-hybrid and AlphaFold2 predicts that they could form a heterodimer. Previously described CE proteins often form multimers of higher orders than two. For example, SYCE2-TEX12 form tetramers and can further assemble into fibers that could form the midline structure of the SC[27]. SYCE3 self-assembles in tetramers that can form higher order structures[39]. When AlphaFold2 was run with different stoichiometries of SCEP1 and SCEP2, heteromeric assemblies were systematically preferred over homomeric ones and none of the Alphafold2 predictions suggested a model including homo and heterodimers. The hetero tetramer model of SCEP1 and SCEP2 in a 2:2 stoichiometry resulted in a complex interlaced assembly (Supplementary Figure 4), suggesting how multimers of a higher order could be formed. We also observed that even if the two proteins are very often found to colocalize they may show some differences, with SCEP1 that seems to encompass SCEP2 at some positions. This result suggests that SCEP1 and SCEP2 do not solely form a parallel dimer nor a tetramer, but possibly a more complex structure with SCEP2 homodimers or multimers at the center connected directly or indirectly to SCEP1 homodimers or multimers nearby. We could hypothesize that additional proteins or protein modifications could be involved to strengthen these interactions. Alternatively, even if the polyclonal antibodies were raised against full length proteins, they may preferentially label part of the proteins leading to a misinterpretation of their relative localization. Further

analyses including structural biochemistry and super resolution microscopy with a series of specific antibodies will be needed to infer the structure that the SCEP1-SCEP2 complex adopts.

In *scep1* or *scep2* mutants, no trace ZYP1 was detected on the SC, which strongly suggests that SCEP1 and SCEP2 are needed for the assembly of TFs. In other species, CE subcomplexes play different roles in SC assembly. In the absence of SYCE2 or TEX12 in mice, or Ecm11 or Gmc2 in budding yeast, chromosomes align, and the TF protein SYCP1 or Zip1 localizes at synapsis initiation sites but synapsis does not extend[20,40,41]. In the absence of SYCE1 or SIX6OS1 or SYCE3 in mice, there are no initiation synapsis sites, and SYCP1 loads on AE in a discontinuous pattern but is unable to form head-to-head polymers[14,16,42]. Therefore, as no SC initiation is observed in *scep1* and *scep2* mutants, the SCEP1-SCEP2 dimer seems to be functionally closer to the mouse SYCE1-SIX6OS1 rather than to SYCE2-TEX12/Ecm11-Gmc2. Moreover, Ecm11 and TEX12 interact with Zip4 and TEX11 (the mice ortholog of the budding yeast Zip4)[26] and we did not detect any interaction between ZIP4 and SCEP1 or SCEP2 even though the Zip4 protein motif involved in this interaction is conserved in *Arabidopsis thaliana*. Other CE proteins, not yet identified, could play the role of SYCE2-TEX12 /Ecm11-Gmc2.

The similarity in ZYP1, SCEP1 and SCEP2 localizations at the center of the SC, the interdependence of each of the three proteins on the two others for their presence on the SC, the perfect similarity between *zyp1, scep1* and *scep2* mutant phenotypes, suggest that they could form a complex. However, no interactions were detected between the SCEP1-SCEP2 dimer and ZYP1, both through yeast two-hybrid and AlphaFold2. A possible reason could be the poor ZYP1 structure prediction by AlphaFold2. Instead of the extended linear coiled-coil protein clearly demonstrated in biochemical and cytological studies with the N-terminal part and C terminal part on opposite sides, AlphaFold2 computes a folding in the middle of the protein between two coiled-coil domains leading to a proximity of the N and C-terminus parts. We were also unable to detect any interaction by yeast two-hybrid both with full length and with truncated proteins. Nevertheless, in other species, not all CE subcomplexes have been shown to interact with their corresponding TF proteins. In mice, SYCE3 interacts with SYCP1 by yeast two-hybrid but not SYCE1, SYCE2, TEX12 or SIXOS1[25]. In yeast, no interaction was found between either Ecm11 or Gmc2 and Zip1 by co-immunoprecipitation (Co-IP) or yeast two-hybrid[26]. In *C. elegans*, SYP-2 and SYP-3 interact with SYP-1 by yeast two-hybrid but not SYP-4[18] whereas Co-IP analyses have shown that two complexes are formed, one containing SYP-5, and the other SYP-6, with SYP-5 and SYP-6 interacting with SYP1 and SYP3 but not with

SYP-4 and SYP-2[10]. Recently, the SC structure has been revisited and, what was thought to be a fixed simple ladder like structure with a few structural proteins is now thought to be more dynamic and includes a series of regulatory protein complexes[10,43]. In both yeast and worms, the central region of the SC, but not the axes, appears to have fluid-like properties[43], where the weakly bound proteins can move within the structure. We can therefore hypothesize that the SCEP1-SCEP2 complex interacts only transiently with ZYP1 and that further analyses would be needed to reveal these interactions. Alternatively, protein modifications may be needed to mediate interactions within the SC. In *S. cerevisiae*, Zip1 and the two CE proteins Ecm11 and Gmc2 have been found to be highly sumoylated and Ecm11 sumo modification is needed for SC polymerization[20,44,45]. In mice, SUMO modifications decorate axes and SC central regions along chromosomes, and inhibiting SUMO conjugation causes synapsis defects[46]. Alternatively, one or more yet unidentified *Arabidopsis* proteins could mediate the interactions between the TFs and the CE proteins SCEP1 and SCEP2.

In budding yeast, mice, *C. elegans*, *Drosophila* or *Sordaria Macrospor*a[7,11,17,47–49], the TF protein is required for class I CO formation. By contrast, in the absence of TFs in rice and *Arabidopsis*, a clear increase in the number of ZMM-promoted COs is observed[4,5,50], but they completely lose interference and the obligatory CO is lost. Thus, COs are randomly distributed among bivalents, explaining why even with a 50% increase in COs, COs form in excess in some bivalents whereas other bivalents do not receive a single CO, producing univalents that segregate randomly at the first meiotic division. In the *scep1* mutant, the number of COs showed a comparable increase to that of *zyp1*[4,5], and they did not exhibit interference. This further supports the conclusion that the tripartite synaptonemal complex itself is essential to impose CO interference in Arabidopsis. Our data are compatible with the "coarsening" model proposed recently in *Arabidopsis* and *C. elegans* where the TF would provide an interface acting as a "railway" on which the ZMM pro-CO factors, such as HEI10, diffuse along, and binds to recombination intermediate sites[51,52–55]. A different rate of association and dissociation from recombination sites creates a local accumulation of HEI10 at a few sites that will become COs at the expense of neighboring sites leading to CO interference. In *scep1*, the TFs are not formed, and as proposed for *zyp1* mutants, HEI10 is not constrained on the SC, HEI10 binds to recombination intermediates and coarsens at the expense of the nucleoplasm pool allowing COs to be formed closed by [51,52–55]. In this coarsening model, heterochiasmy relies on the size of the SC which is smaller in *Arabidopsis*

female meiosis and thus accumulates less HEI10 foci than in male meiosis which has a longer SC. In the absence of the ZYP1 "railway", the SC is no longer the metric for the HEI10 dynamic and heterochiasmy is not maintained in *scep1*$^{-/-}$, just as in *zyp1-1*[4].

Orthologs of SCEP1 and SCEP2 have been found in all the species or at least in one representative species of the various families of vascular plants, except in gymnosperms. Outside Tracheophytes, no convincing homologs were detected. However, a recent study[38] detected ZYP1 in all the lineages of Viridiplantae including gymnosperms. Our data suggest that the three proteins SCEP1, SCEP2 and ZYP1 form a functional triad and could therefore be expected to be found together. As potential, although unsure, ZYP1 homologs could be identified in the species without SCEP1 or SCEP2 homologs, it can be hypothesized that SCEP1 and SCEP2 homologs do exist but exhibit high sequence divergence compared to the *Arabidopsis* SCEP1 and SCEP2 sequences. In this scenario, all known SC proteins may derive from common ancestors, but sequence divergence makes them unrecognizable with the actual tools used for sequence similarity analyses. Alternatively, TF and/or CE proteins could have emerged independently during evolution, and selected on their 3D structure to assemble and synapse chromosomes. Further homology searches based on the structure of these proteins may shed a clearer light on the composition of the central region of these species.

Methods

Plant materials and growth conditions

Arabidopsis thaliana plants were grown in greenhouses with 70% humidity and under a 16h/8h day/night photoperiod with temperatures 19°C day and 16°C night. Wild-type Col-0 and Ler-1 are 186AV1B4 and 213AV1B1 from the Versailles *A. thaliana* stock center (http://publiclines.versailles.inra.fr/). The *zyp1-1* mutant was described previously [4]. *scep1-1/scep1-7*, heterozygous *scep1-1*$^{+/-}$ plants were crossed with heterozygous *scep1-7*$^{+/-}$ plants to produce *scep1-1/scep1-7* heteroallelic homozygous mutant. These plants were backcrossed as male or female with wild-type Col to generate the sequencing populations. Backcross populations were treated as described [51]. The four T-DNA insertion lines in *AT3G28370* were provided by NASC (http://nasc.nott.ac.uk/). Neither the line before the ATG (PST16975) nor

the two lines with an insertion in the last intron (N525173, N508352) that are predicted to only remove the last five amino acids of the long isoform (Extended Data Figure. 1E-F) showed any univalent on at least 50 different metaphase I meiotic cells. The line N663933 (*scep2-1*) was further characterized. To generate the double homozygous *scep1-1*$^{-/-}$ *scep2-1*$^{-/-}$, heterozygous *scep1-1*$^{+/-}$ and *scep2-1*$^{+/-}$ plants were crossed. The obtained double heterozygous *scep1-1*$^{+/-}$ *scep2-1*$^{+/-}$ were selfed to produce double homozygous *scep1-1*$^{-/-}$ *scep2-1*$^{-/-}$, single mutants *scep1-1*$^{-/-}$ and *scep2-1*$^{-/-}$ and wild type plants. These sister plants were used to perform MLH1 foci counting. Double homozygous plants *scep1-1*$^{-/-}$ *zyp1-1*$^{-/-}$ and *scep2-1*$^{-/-}$ *zyp1-1*$^{-/-}$ were obtained after crossing heterozygous plants for each mutation. After selfing double mutants were selected. Genotyping conditions used in that study are listed in Supplementary Table 3.

Expression data

Transcriptomic data were downloaded from https://datacommons.cyverse.org/browse/iplant/home/araport/rnaseq_bam/Klepikova and analyzed using an in-house R script. The data was filtered to retain only the expression levels in flower (stages 1 through 19 corresponding to buds from under 0.3 mm to more than 3 mm as defined in[30]). Differential gene expression analysis was performed with the edgeR package and the normalization was done by the trimmed mean of M-values method (TMM). As known meiotic genes displayed a peak expression at stage 15 (buds between 0.3 and 0.5 mm), genes that had a mean value at stage 15 (buds between 0.3 and 0.5 mm) at least 1.8 times higher than the mean values at stages 1 (buds > 3mm), 2 (buds between 2.6 and 2.9 mm), and 3 (buds between 2.1 and 2.5 mm), and where the mean value at stage 15 (buds between 0.3 and 0.5 mm) was the highest among all other flower stages were selected corresponding to almost 250 genes. To narrow down the number of genes obtained making the screen doable, genes that had an expression level above that of *DMC1* and below *SPO11-2* (the most and least expressed meiotic genes) were filtered out and the 80 genes exhibiting a mean root expression level lower by at least 30% than that observed during the flower stage 15 (buds between 0.3 and 0.5 mm) were retained.

RT-PCR experiments

Total RNA extracted from flower buds were prepared and purified using the RNeasy Plant Mini Kit (Qiagen) according to the manufacturer's instructions. cDNAs were synthesized out of 1µg

of total RNA using an oligo-dT18 primer and RevertAid RT Reverse Transcription Kit (ThermoFisher Scientific) according to the manufacturer's instructions. cDNAs were used to amplify the 3' extremity of SCEP1 (RT_SCEP1_fwd/RT_SCEP1_rev) or SCEP2 (RT_SCEP2_fwd/RT_SCEP2_rev1 or RT_SCEP2_fwd/RT_SCEP2_rev2). PCR fragments were Sanger sequenced (Genoscreen, Lille, France).

Generation of the CRISPR-Cas9 *scep1* mutants

Three guide RNAs targeting the *AtSCEP1* gene (*At1g10710*) were designed with the CRISPOR (http://tefor.net/crispor/crispor.cgi)[56]. Expression cassettes sgRNA_SCEP1#1, sgRNA_SCEP1#2, and sgRNA_SCEP1#3 including Gateway recombination sites were synthesized by Twist Biosciences (San Francisco, CA) and inserted in the pDE–Cas9–DSred vector [57,58] by LR reaction using the Gateway™ technology (Invitrogen). The resulting construct was transformed into *A. thaliana* ecotype Columbia (Col-0) plants or Lansdberg *erecta* (Ler) plants using the floral dip method [59]. Plant transformants (T1) were selected by seed fluorescence and twenty transformants were transferred to the greenhouse. The progeny without fluorescence were selected and screened for mutations by PCR amplification (SCEP1_RP1/ SCEP1_LP1 or SCEP1_RP2/ SCEP1_LP2) and Sanger sequencing at the targeted locus. Seven independent lines carrying homozygous frameshift mutations were used for further characterization.

Yeast two hybrid assays

The DNA sequence corresponding to SCEP1 and 217 first amino acids of SCEP2 and the last 469 amino acids of ZIP4 were chemically synthesized (Twist Biosciences). attB1 and attB2 recombinant tails were added to these fragments in order to transfer them into the pDONOR207 using the Gateway™ technology (Invitrogen). Truncations of SCEP1 or SCEP2 were generated by PCR using specific primers flanking attB1 and attB2 recombination sites and cloned into pDONOR207. After sequencing, the entry vectors were used to generate the appropriate pGAD and pGBK yeast two hybrid expression vectors. These were transformed into AH109 and Y187 strains respectively by heat shock, and grown on selective media (without leucine for transformed AH109 and without tryptophan for transformed Y187). Conjugations were carried out in liquid non-selective media overnight, and then grown on solid media lacking both leucine and tryptophan (SD-LW). Each interaction was tested by

taking 8 separate yeast colonies grown on SD-LW and resuspending them in 8 separate 100 µl water wells. 10 µl of these were then successively deposited on solid SD-LW, SD-LWH (SD-LW without histidine) and SD-LWHA (SD-LWH without adenine). Two proteins were deemed to interact when the 8 separate colonies grew on SD-LWH and/or SD-LWHA and no self-activation could be observed.

The DNA sequence corresponding to the 416 first amino acids of ZYP1a (ZYP1aNter) or the 469 last amino acids of ZYP1a (ZYP1aCter) were chemically synthesized (Twist Biosciences). attL1 and attL2 recombinant tails were added to these fragments in order to transfer them directly into the yeast two hybrid expression vectors using the Gateway™ technology (Invitrogen). Details on the constructs are provided in Supplementary Table 4.

To simplify visualization of the interaction results, a scoring of each protein pair is used, called the InterRatio. This ratio reflects the number of times an interaction is observed with respect to the number of times it was tested. Interactions observed due to self-activation are not considered, and only interactions that also grew on the LW medium are considered. To fit the data collected, a weighting is done to reflect whether the interaction was observed on LWHA or only on LWH, the latter reflecting a weaker interaction.

$$InterRatio = \frac{n(LWHA) + \frac{1}{2}n(LWH)}{n(Tests)}$$

Here, *n(LWHA)* is the number of times the interaction is observed on the LWHA medium, *n(LWH)* the number of times the interaction is observed only on the LWH medium (meaning not on the LWHA medium), and *n(Tests)* is the number of times the interaction was tested (always greater than 0). For example, for an interaction between two proteins A and B that show no self-activation and for which two interaction tests were performed, one showing an interaction on LWH and LWHA while the second test only showed interaction on the LWH medium, the InterRatio takes a value of $\frac{1+\frac{1}{2}\times 1}{2} = 0.75$. This is only computed because the yeasts also grew on the LW medium. The InterRatio is computed in an R script that takes Supplementary Table2 as its input and produces the corresponding Inter Ratio heatmap.

AlphaFold2 predictions

AlphaFold2 predictions of both monomers and multimers were computed through the ColabFold notebook (ColabFold v1.3 and AlphaFold2 v2.2) using a ColabPro+ plan

(https://colab.research.google.com/github/sokrypton/ColabFold/blob/main/AlphaFold2.ipynb). The plDDT, PAE, and ipTM scores and graphs were provided directly by this notebook [60]. Predicted structures were not relaxed using amber, and no template information was used. mmseqs_uniref_env was used for the unpaired MSA, and sequences from the same species were paired. For the advanced settings, the automatic modes were applied, only one seed was used and dropouts were not enabled. Images were produced using UCSF ChimeraX [61].

Production of anti SCEP1, SCEP2 or ZYP1-Cter antibodies

The cDNA of SCEP1 or SCEP2 inserted in pDONOR207 were transferred into the expression plasmid pDEST17 (Novagen) using the Gateway™ technology (Invitrogen). Resulting plasmids were used to transform the *E. coli* expression strain BL21 ER2566 (New England Biolabs). Protein expression was induced at 37°C for 3h and recombinant protein was resolubilized as described in [62]. Rabbit anti-SCEP1 or rat anti-SCEP2 antibodies were obtained (Eurogentec) and used at a dilution 1:200 for immunofluorescence. The ZYP1 polyclonal Cter antibody (Lab name: PAK133) was produced against the peptide CEGSLNPYADDPYAFD which is located at the very C-terminus end of the ZYP1 proteins. It was raised in rabbit and affinity purified using the 28-day program of Eurogentec.

Cytology

Seeds were counted after silique clearing in 70% ethanol. Meiotic chromosome spreads were DAPI stained as described previously [63]. For each genotype, DAPI staining was performed on spreads obtained from pooled anthers from 10 to 20 flowers on one plant for *scep1-1, scep1-2, scep1-3, scep1-4, scep1-5*, two plants for *scep1-6, zyp1-1, scep1-1 scep2-1, scep1-1 zyp1-1, scep2-1 zyp1-1* and 4 plants for wt and *scep1-7*. Immunolocalization was performed either on 2D lipsol male meiotic spreads as described [64] or on 3D preserved cells as described[31,51]. For immunostaining, eight primary antibodies were used for both epifluorescence and super resolution microscopy: anti-REC8 raised in rat or in rabbit [65] (dilution 1:250), anti-MLH1 in rabbit [62] (dilution 1/1000), anti-HEI10 in chicken (dilution 1/10000) [51], anti-ASY1 in guinea-pig [31](dilution 1/250), anti-ZYP1 in rat [3] (dilution 1/250), anti-ZYP1-Cter PAK133 in rabbit (dilution 1/200, this study), anti-SCEP1 in rabbit (dilution 1/200, this study) and, anti-SCEP2 in rat (dilution 1/200, this study). Secondary antibodies were conjugated with Alexa 488, Alexa 568,

or Alexa 647 for epifluorescence and Abberior STAR Red (1/500), or STAR Orange (1/500) for STED microscopy (Supplementary Table 12).

Images were taken using a Zeiss Axio Observer microscope. MLH1 immunofluorescence studies were carried out on 3D preserved meiocytes as described [31]. Super-resolution images were acquired using the Abberior STEDYCON system. Super-resolution images were acquired with the Abberior instrument facility line (https://abberior-instruments.com/) 561- and 640-nm. excitation lasers (for STAR Orange and STAR Red, respectively) and a 775-nm STED depletion laser. Confocal images were taken with the same instrument with a 485-nm excitation laser (for STAR GREEN/Alexa488).

Image processing and analysis

Deconvolution of the images was performed by Huygens Essential (version 21.10, Scientific Volume Imaging, https://svi.nl/) using the classic maximum likelihood estimation algorithm with lateral drift stabilization; signal-to-noise ratio: 7 for STED images and 20 for confocal images, 40 iterations, and quality threshold of 0.5. Maximum intensity projections and contrast adjustments were also done with Huygens Essential 22.04.0p0 64b. Deconvoluted pictures were imported into Imaris x64 9.6.0 (https://imaris.oxinst.com/, Oxford Instruments, UK) for subsequent analysis. MLH1 foci were counted in diplotene and diakinesis cells. The vast majority of MLH foci colocalize with a HEI10 focus. Only double MLH1/HEI10 foci present on chromosomes were taken into account.

For measuring distances between REC8-labelled axial bridges, 10 independent cells (four for each mutant and two for the wild type) and 25 counts were recorded. Lines (width=3) were drawn on random seemingly flat regions using ImageJ. For each line, the grey-scale intensity profile was exported from ImageJ and analyzed in R. The lines were then individually fitted using a local polynomial regression (loess function - stats package) with a span of 0.5. The x-values of the two local maxima given by the fitted values were recorded for each line, and the distance between the two axes was deduced. Since homologous chromosomes in mutants were never fully aligned, the lines were drawn on regions where chromosomes were the closest “by eye” to each other. Overall distance between homologous chromosomes in mutants is therefore underestimated.

The same strategy was used to calculate the distance between occasional SCEP1 double lines and between the ZYP1 C-terminus section.

606
607
608 **CO analysis**
609 The previously described method was followed for generation of high-confidence SNP
610 markers between Col and Ler, mapping of sequencing reads, meiotic CO prediction, and
611 filtering of the poorly covered and potentially contaminated samples [4,35,51,66,67]. Then,
612 identified COs were manually and randomly checked by using inGAP-family [66]. A total of 937
613 and 1,077 COs were identified from the 142 and 143 *scep1* female and male plants
614 (ArrayExpress number E-MTAB-12985), respectively. The list of 1,192 and 1,587 COs of the
615 wild type female and male populations (428 and 294 plants, ArrayExpress number E-MTAB-
616 11254), and the list of 1,933 and 1,596 COs of the *zyp1* female and male populations (272 and
617 225 plants, ArrayExpress number E-MTAB-9593, E-MTAB-11696) from the previous studies
618 [4,35,51] were used for the analysis of CO number and distribution, and crossover interference,
619 following the previous description [4,51]. The list of CO positions can be found in Supplementary
620 Table 7. Raw read data of Fig. 7 can be found in the EBI ArrayExpress database under accession
621 number E-MTAB-12985 https://www.ebi.ac.uk/biostudies/studies/E-MTAB-12985.
622
623 **SCEP1 and SCEP2 orthologs**
624 *Arabidopsis* protein sequences from SCEP1 (AT1G33500), SCEP2 (AT3G28370), and ZYP1b
625 (AT1G22275) were taken from the TAIR website, while protein sequences from other species
626 were taken from the NCBI accessions. NCBI PSI-BLASTs against *Viridiplantae* were used to
627 search for SCEP1 and SCEP2 homologs, with an E-value threshold of 5e-3 and BLOSUM62
628 matrix. Two iterations were performed, and proteins with an E-value less than 10e-10 and a
629 percent identity greater than 10% were considered potential homologs. In addition, proteins
630 that were smaller than 100 amino acids and larger than 500 were also filtered out. The same
631 strategy was used for ZYP1, but a single iteration was performed and proteins below 450
632 amino acids were discarded. Lowering the E-value threshold for homolog consideration to 5e-
633 3 did not modify the results shown in Figure 8. A description of the homologs can be found in
634 Supplementary Table 6. A reciprocal best-hit strategy with identical BLAST parameters was
635 used to confirm the presence of homologs in *Selaginella moellendorffii, Amborella trichopoda*,
636 *Jatropha curcas*, *Solanum lycopersicum,* and *Gossypium raimondii.* The PSI-BLASTs targeted at
637 individual species from Figure 8 for which no SCEP1, SCEP2, and/or ZYP1 homolog had initially

been found were performed with identical parameters. PSI-BLAST results were downloaded and analyzed using in-house R scripts to filter and rank homologs, quantify their presence or absence in the different species, fetch the protein sequences, draw the phylogenic tree and the associated matrix. The phylogenic tree was taken from [68], from which a subset of *Viridiplantae* was made. The two gymnosperms and *Marchantia* were added according to NCBI taxonomy and the phylogeny proposed by [69,70]. No phylogenic tree prediction was made in our analysis; only the presence or absence of SCEP1, SCEP2, and ZYP1 in major plant species was investigated.

Data availability

Raw read data of Fig. 7 can be found in the EBI ArrayExpress database under accession number E-MTAB-12985 https://www.ebi.ac.uk/biostudies/studies/E-MTAB-12985.

Acknowledgments

We wish to thank Lyna Iguertsira and Zoé Klising for technical help with plasmid construct and fertility characterization, and Delphine Charif for bioinformatic guidance in the analysis of transcriptomic data. This work has benefited from the support of the IJPB's Plant Observatory technological platforms. This research was funded by ANR (COPATT ANR-20-CE12-0006), by core funding from the Max Planck Society and an Alexander von Humboldt Fellowship to Q.L. The IJPB benefits from the support of Saclay Plant Sciences-SPS (ANR-17-EUR-0007).

Author contributions

N.V. produced all the genetic material, analyzed the fertility data, produced and analyzed the *scep1-/- alleles*, produced the SCPE1 and SCEP2 proteins to obtain antibodies, produced and analyzed the immunocytology data at standard resolution. M.P. analyzed the localization and distances between SC components, analyzed the Alphafold2 data and produces and analyzed the SCEP1 and SCEP2 orthologs data. S.D. produced and analyzed the STED immuocytology data. Q.L. analyzed the sequencing data and performed recombination, and interference, and aneuploidy analyses. A.C., A.H., J.G. produced the MLH1and HEI10 immunocytology data. R.G. produced the first analysis of the SCEP1-SCEP2 complex with Alphafold2. M.G. and R.M. contributed to the supervision and analysis of the cytological and genetic data. C.M. lead the

project, produced the bioinformatic analysis of the transcriptomic data and wrote the manuscript with input from all co-authors.

Competing interests

The authors declare no competing interests

Figure legends

Figure 1. Identification and characterization of SCEP1 and SCEP2
(a) Expression profile of 28 known meiotic genes (Supplementary Table 1) in buds of various sizes including *SCEP1* in red and *SCEP2* in green. **(b)** DAPI staining of chromosomes in male meiosis at metaphase I or metaphase II in wt, *scep1*-1 and, *scep2*-1. White arrows: univalents. Scale bar 5µm. **(c)** Quantification of univalents at metaphase I. Number of cells in brackets. **(d)** Structure obtained from the TAIR figuring the introns and exons of the *SCEP1* and *SCEP2* genes. The position of the gRNA (green) used for CRISPR-Cas9 in *SCEP1* are placed above the gene structure and the position of the mutant alleles are indicated below the gene structure. The position of the T-DNA insertion in *SCEP2* is indicated below the gene structure. **(e)** Predicted structure of SCEP1 or SCEP2 from AlphaFold2 with colored by per-residue pLDDT scale. High pLDDT values indicate strong confidence in the predicted structure, and low values indicate low confidence. SCEP1 and SCEP2 protein sequences were deduced after sequencing cDNAs. Two different putative proteins were found for SCEP2 that differ by the last 50 amino acids (see material and methods, Extended data Figure1). **(f)** Mean number of seeds per silique. Numbers of plants and siliques in Supplementary Table 8. Tukey's multiple comparison test.

Figure 2. ZYP1s is not loaded in *scep1* and *scep2* mutants
(a) Immunolocalization of ZYP1 and ASY1 in wild-type, *scep1-1* and *scep2-1* male meiocytes (standard resolution microscopy). Scale bar 2µm. **(b)** Immunolocalisation of ASY1 (green) and REC8 (magenta) in wild-type, *scep1-1* and *scep2-1* male meiocytes analyzed with STED microscopy. Scale bar: 5 µm. **(c)** Comparison of lateral distances between REC8 axes in wild-type, *scep1-1* and *scep2-1* mutants. Tukey HSD test, p-values between groups a and b: $p < 10^{-4}$.

Figure 3. SCEP1 and SCEP2 are loaded on the SC central region
(a) Immunolocalization of ASY1 (magenta) and SCEP1 (green) on wild-type male meiocytes analyzed by standard resolution microscopy. Leptotene (top row) zygotene (middle row) pachytene (bottom row). Scale bar 2 µm. **(b)** Immunolocalization of ASY1 (magenta) and SCEP2 (green) on wild-type male meiocytes analyzed by standard resolution microscopy. Leptotene (top row) zygotene (middle row) pachytene (bottom row). Scale bar 2 µm. **(c)** Immunolocalization of ZYP1s (magenta) and SCEP1 (green) on wild-type male meiocytes at zygotene (upper) or pachytene (middle) analyzed by standard resolution microscopy. Lower panel show an enlarged vision from the dotted box. Scale bar 2 µm. **(d)** Immunolocalization of ZYP1s (magenta) and SCEP2 (green) on wild-type male meiocytes at zygotene (upper) or pachytene (middle) analyzed by standard resolution microscopy. Lower panels show an enlarged vision from the dotted box. Scale bar 2 µm.

Figure 4. SCEP1 and SCEP2 colocalize at the center of the SC

(a) Immunolocalization of REC8 (magenta) and SCEP2 (blue) on wild-type male meiocytes analyzed with STED microscopy. Scale bar 2 µm. **(b)** Immunolocalization of ZYP1 C-ter (magenta) and SCEP2 (blue) on wild-type male meiocytes analyzed with STED microscopy. Scale bar 2 µm. **(c)** Immunolocalization of REC8 (magenta) and SCEP1 (blue) on wild-type male meiocytes analyzed with STED microscopy. Scale bar 2 µm. **(d)** Immunolocalization of SCEP1 (magenta) and SCEP2 (blue) on wild-type male meiocytes analyzed with STED microscopy. Scale bar 2 µM. **(e)** Comparison of lateral distances between observed SCEP1 lines (when applicable), ZYP1 Cter lines (PAK133 antibody) and REC8 lines in wild-type plants. (black dot: mean; vertical black line : SD). Tukey HSD test, *: $p < 0.01$, ****: $p < 10^{-4}$.

Figure 5. The three proteins SCEP1, SCEP2 and ZYP1 are needed to assemble the SC central region.

Immunolocalization of ASY1 in magenta and SCEP1 **(a)**, SCEP2 **(b)** in green was performed on spread male meiocytes from wild-type, *scep1-1, scep2-1* or *zyp1-1* mutants. Scale bar 2 µm.

Figure 6. SCEP1 and SCEP2 form a complex

(a) 3D model of SCEP1-SCEP2 built using AlphaFold2 structure prediction program. Top: SCEP1 and SCEP2 are represented as pink and blue cartoons, respectively. Bottom: the SCEP1-SCEP2 complex colored by per-residue pLDDT. High and low pLDDT values indicate strong and low confidence in the predicted structure, respectively. Predicted Aligned Error (PAE) values for the SCEP1-SCEP2 dimer. Low PAE values indicate strong confidence in the distances between two amino acids, and high values indicate low confidence. **(b)** Constructs of SCEP1, SCEP2, ZYP1A and ZIP4 used for the yeast two-hybrid assays. Heatmap of the yeast two hybrids interactions. The InterRatio is detailed in Material and Methods. Red: interaction seen on the most stringent media, light yellow: no interaction observed. The number in the tiles refer to the number of repetitions of the assay. AD: fusion of protein sequence to yeast two hybrid activating domain, BD: fusion of protein sequence to yeast two hybrid DNA binding domain.

Figure 7: MLH1 foci and COs are increased in CE mutants

(a) MLH1–HEI10 foci were quantified following a triple immunolocalization ASY1–MLH1–HEI10 performed on wt (n=184), *scep1-1* (n=93)*, scep2-1* (n=114) and *scep1-1 scep2-1* (n=72) male meiocytes and imaged with an epifluorescence microscope. Each dot is an individual cell, and the bar is the mean**.** Tukey's multiple comparison test. Only p-values < 0.01 are shown (Supplementary Table 10)**.** (**b**) The number of COs detected following whole-genome sequencing of female and male backcrosses of Col/L*er* F1 hybrids. Each dot is an individual BC1 plant, the mean value of each population is indicated on the top and the population size is shown in brackets. The two-sided Mann–Whitney test was used to evaluate the differences in CO numbers. (**c**) Distribution of inter-CO distances for chromosomes having exactly two COs. The gray bars represent the expected distribution of COs in the absence of interference, as calculated by permuting the CO positions between gametes. The number of analyzed events and the p-value from the Mann–Whitney test comparing observed and expected distributions are indicated in brackets. (**d**) Chromosomes were divided into 15 intervals, and the mean Coefficient of Coincidence (CoC) was calculated for pairs of intervals separated by a certain distance (Mb). (**e**) The distribution of COs along chromosome 1 in female and male wild type, *zyp1* and *scep1-1*. Other chromosomes are presented in Extended Data Fig. 3. The

centromere and pericentromeric regions are indicated by gray and blue shading, respectively. The analysis is done with 1-Mb windows and 50-kb sliding steps. For pericentromeric regions and each non-overlapping 1-Mb window along chromosome arms, Pearson's Chi-squared Test was used to examine the difference between wild type and *scep1-1*. Windows with p-value (corrected with the FDR method) < 0.05 were marked by stars.

Figure 8: SCEP1, SCEP2 and ZYP1 homologs can be found in all major angiosperm species. The heatmap indicates the presence or absence of SCEP1, SCEP2 or ZYP1 homologs determined through a PSI-BLAST approach. An additional classification of "unsure" homologs was added, see Materials and Methods. *Viridiplantae* phylogenetic tree adapted from[68].

References

1. Zickler, D. & Kleckner, N. Recombination, Pairing, and Synapsis of Homologs during Meiosis. *Cold Spring Harb. Perspect. Biol.* **7**, a016626 (2015).
2. Schmekel, K. *et al.* Organization of SCP1 Protein Molecules within Synaptonemal Complexes of the Rat. *Exp. Cell Res.* **226**, 20–30 (1996).
3. Higgins, J. D., Sanchez-Moran, E., Armstrong, S. J., Jones, G. H. & Franklin, F. C. H. The Arabidopsis synaptonemal complex protein ZYP1 is required for chromosome synapsis and normal fidelity of crossing over. *Genes Dev* **19**, 2488–2500 (2005).
4. Capilla-Pérez, L. *et al.* The synaptonemal complex imposes crossover interference and heterochiasmy in Arabidopsis. *Proc. Natl. Acad. Sci. U. S. A.* **118**, 1–11 (2021).
5. France, M. G. *et al.* ZYP1 is required for obligate cross-over formation and cross-over interference in Arabidopsis. *Proc. Natl. Acad. Sci. U. S. A.* **118**, 1–11 (2021).
6. Sym, M., Engebrecht, J. A. & Roeder, G. S. ZIP1 is a synaptonemal complex protein required for meiotic chromosome synapsis. *Cell* **72**, 365–378 (1993).
7. Vries, F. A. T. D. *et al.* Mouse Sycp1 functions in synaptonemal complex assembly, meiotic recombination, and XY body formation. *Genes Dev* **19**, 1376–1389 (2005).
8. MacQueen, A. J., Colaiacovo, M. P., McDonald, K. & Villeneuve, A. M. Synapsis-dependent and -independent mechanisms stabilize homolog pairing during meiotic prophase in C. elegans. *Genes Dev* **16**, 2428–2442 (2002).
9. Hurlock, M. E. *et al.* Identification of novel synaptonemal complex components in C. Elegans. *J. Cell Biol.* **219**, (2020).
10. Zhang, Z. *et al.* Multivalent weak interactions between assembly units drive synaptonemal complex formation. *J. Cell Biol.* **219**, (2020).
11. Page, S. L. & Hawley, R. S. c(3)G encodes a Drosophila synaptonemal complex protein. *Genes Dev* **15**, 3130–3143 (2001).
12. Dong, H. & Roeder, G. S. Organization of the yeast Zip1 protein within the central region of the synaptonemal complex. *J Cell Biol* **148**, 417–426 (2000).
13. Costa, Y. *et al.* Two novel proteins recruited by synaptonemal complex protein 1 (SYCP1) are at the centre of meiosis. *J Cell Sci* **118**, 2755–2762 (2005).
14. Schramm, S. *et al.* A Novel Mouse Synaptonemal Complex Protein Is Essential for Loading of Central Element Proteins, Recombination, and Fertility. *PLoS Genet.* **7**, e1002088 (2011).
15. Hamer, G. *et al.* Characterization of a novel meiosis-specific protein within the central element of the synaptonemal complex. *J Cell Sci* **119**, 4025–4032 (2006).
16. Gómez-H, L. *et al.* C14ORF39/SIX6OS1 is a constituent of the synaptonemal

808 complex and is essential for mouse fertility. *Nat. Commun.* **7**, 13298 (2016).
809 17. Colaiacovo, M. P. *et al.* Synaptonemal complex assembly in C. elegans is dispensable
810 for loading strand-exchange proteins but critical for proper completion of recombination. *Dev*
811 *Cell* **5**, 463–474 (2003).
812 18. Smolikov, S., Schild-Prufert, K. & Colaiacovo, M. P. A yeast two-hybrid screen for
813 SYP-3 interactors identifies SYP-4, a component required for synaptonemal complex
814 assembly and chiasma formation in Caenorhabditis elegans meiosis. *PLoS Genet* **5**, e1000669
815 (2009).
816 19. Smolikov, S. *et al.* SYP-3 restricts synaptonemal complex assembly to bridge paired
817 chromosome axes during meiosis in Caenorhabditis elegans. *Genetics* **176**, 2015–2025
818 (2007).
819 20. Humphryes, N. *et al.* The Ecm11-Gmc2 Complex Promotes Synaptonemal Complex
820 Formation through Assembly of Transverse Filaments in Budding Yeast. *PLoS Genet.* **9**,
821 e1003194 (2013).
822 21. Page, S. L. *et al.* Corona is required for higher-order assembly of transverse filaments
823 into full-length synaptonemal complex in Drosophila oocytes. *PLoS Genet* **4**, e1000194
824 (2008).
825 22. Collins, K. A. *et al.* Corolla Is a Novel Protein That Contributes to the Architecture of
826 the Synaptonemal Complex of *Drosophila*. *Genetics* **198**, 219–228 (2014).
827 23. Ur, S. N. & Corbett, K. D. Architecture and Dynamics of Meiotic Chromosomes.
828 *Annu. Rev. Genet.* **55**, 497–526 (2021).
829 24. Zhang, F. G., Zhang, R. R. & Gao, J. M. The organization, regulation, and biological
830 functions of the synaptonemal complex. *Asian J. Androl.* **23**, 580–589 (2021).
831 25. Crichton, J. H. *et al.* Structural maturation of SYCP1-mediated meiotic chromosome
832 synapsis by SYCE3. *Nat. Struct. Mol. Biol.* **30**, 188–199 (2023).
833 26. Pyatnitskaya, A., Andreani, J., Guérois, R., De Muyt, A. & Borde, V. The Zip4 protein
834 directly couples meiotic crossover formation to synaptonemal complex assembly. *Genes Dev.*
835 **36**, 53–69 (2022).
836 27. Dunce, J. M., Salmon, L. J. & Davies, O. R. Structural basis of meiotic chromosome
837 synaptic elongation through hierarchical fibrous assembly of SYCE2-TEX12. *Nat. Struct.*
838 *Mol. Biol.* **28**, 681–693 (2021).
839 28. Schild-Prüfert, K. *et al.* Organization of the synaptonemal complex during meiosis in
840 Caenorhabditis elegans. *Genetics* **189**, 411–421 (2011).
841 29. Cahoon, C. K. *et al.* Superresolution expansion microscopy reveals the three-
842 dimensional organization of the *Drosophila* synaptonemal complex. *Proc. Natl. Acad. Sci.*
843 **114**, (2017).
844 30. Klepikova, A. V., Kasianov, A. S., Gerasimov, E. S., Logacheva, M. D. & Penin, A.
845 A. A high resolution map of the *Arabidopsis thaliana* developmental transcriptome based on
846 RNA-seq profiling. *Plant J.* **88**, 1058–1070 (2016).
847 31. Hurel, A. *et al.* A cytological approach to studying meiotic recombination and
848 chromosome dynamics in Arabidopsis thaliana male meiocytes in three dimensions. *Plant J.*
849 **95**, 385–396 (2018).
850 32. Jumper, J. *et al.* Highly accurate protein structure prediction with AlphaFold. *Nature*
851 **596**, 583–589 (2021).
852 33. Mirdita, M. *et al.* ColabFold: making protein folding accessible to all. *Nat. Methods*
853 **19**, 679–682 (2022).
854 34. Lambing, C. *et al.* Arabidopsis PCH2 Mediates Meiotic Chromosome Remodeling and
855 Maturation of Crossovers. *PLOS Genet.* **11**, e1005372 (2015).
856 35. Lian, Q. *et al.* The megabase-scale crossover landscape is largely independent of
857 sequence divergence. *Nat. Commun.* **13**, 3828 (2022).

858 36. Muller, H. J. the mechanisms of crossing-over. *Am. Nat* **582**, 193–434 (1916).
859 37. Zickler, D. & Kleckner, N. A few of our favorite things: Pairing, the bouquet,
860 crossover interference and evolution of meiosis. *Semin. Cell Dev. Biol.* **54**, 135–148 (2016).
861 38. Thangavel, G., Hofstatter, P. G., Mercier, R. & Marques, A. Tracing the evolution of
862 the plant meiotic molecular machinery. *Plant Reprod.* (2023) doi:10.1007/s00497-022-00456-
863 1.
864 39. Dunne, O. M. & Davies, O. R. A molecular model for self-assembly of the
865 synaptonemal complex protein SYCE3. *J. Biol. Chem.* **294**, 9260–9275 (2019).
866 40. Bolcun-Filas, E. *et al.* SYCE2 is required for synaptonemal complex assembly, double
867 strand break repair, and homologous recombination. *J Cell Biol* **176**, 741–747 (2007).
868 41. Hamer, G. *et al.* Progression of meiotic recombination requires structural maturation
869 of the central element of the synaptonemal complex. *J Cell Sci* **121**, 2445–2451 (2008).
870 42. Bolcun-Filas, E. *et al.* Mutation of the Mouse Syce1 Gene Disrupts Synapsis and
871 Suggests a Link between Synaptonemal Complex Structural Components and DNA Repair.
872 *PLoS Genet* **5**, e1000393 (2009).
873 43. Rog, O., Köhler, S. & Dernburg, A. F. The synaptonemal complex has liquid
874 crystalline properties and spatially regulates meiotic recombination factors. *eLife* **6**, e21455
875 (2017).
876 44. Leung, W.-K. *et al.* The synaptonemal complex is assembled by a polySUMOylation-
877 driven feedback mechanism in yeast. *J. Cell Biol.* **211**, 785–793 (2015).
878 45. Bhagwat, N. R. *et al.* SUMO is a pervasive regulator of meiosis. *eLife* **10**, e57720
879 (2021).
880 46. Rao, H. B. D. P. *et al.* A SUMO-ubiquitin relay recruits proteasomes to chromosome
881 axes to regulate meiotic recombination. *Science* **355**, 403–407 (2017).
882 47. Borner, G. V. *et al.* Crossover/noncrossover differentiation, synaptonemal complex
883 formation, and regulatory surveillance at the leptotene/zygotene transition of meiosis. *Cell*
884 **117**, 29–45 (2004).
885 48. Smolikov, S. *et al.* Synapsis-defective mutants reveal a correlation between
886 chromosome conformation and the mode of double-strand break repair during Caenorhabditis
887 elegans meiosis. *Genetics* **176**, 2027–2033 (2007).
888 49. Espagne, E. *et al.* Sme4 coiled-coil protein mediates synaptonemal complex assembly,
889 recombinosome relocalization, and spindle pole body morphogenesis. *Proc. Natl. Acad. Sci.*
890 **108**, 10614–10619 (2011).
891 50. Wang, K., Wang, C., Liu, Q., Liu, W. & Fu, Y. Increasing the Genetic Recombination
892 Frequency by Partial Loss of Function of the Synaptonemal Complex in Rice. *Mol. Plant* **8**,
893 1295–1298 (2015).
894 51. Durand, S. *et al.* Joint control of meiotic crossover patterning by the synaptonemal
895 complex and HEI10 dosage. *Nat. Commun* (2022).
896 52. Morgan, C. *et al.* Diffusion-mediated HEI10 coarsening can explain meiotic crossover
897 positioning in Arabidopsis. *Nat. Commun.* **12**, 4674 (2021).
898 53. Fozard, J. A., Morgan, C. & Howard, M. Coarsening dynamics can explain meiotic
899 crossover patterning in both the presence and absence of the synaptonemal complex. *eLife* **12**,
900 e79408 (2023).
901 54. Zhang, L., Köhler, S., Rillo-Bohn, R. & Dernburg, A. F. A compartmentalized
902 signaling network mediates crossover control in meiosis. *eLife* **7**, e30789 (2018).
903 55. Zhang, L., Stauffer, W., Zwicker, D. & Dernburg, A. F. *Crossover patterning through*
904 *kinase-regulated condensation and coarsening of recombination nodules*.
905 http://biorxiv.org/lookup/doi/10.1101/2021.08.26.457865 (2021)
906 doi:10.1101/2021.08.26.457865.
907 56. Concordet, J.-P. & Haeussler, M. CRISPOR: intuitive guide selection for

CRISPR/Cas9 genome editing experiments and screens. *Nucleic Acids Res.* **46**, W242–W245 (2018).
57. Fauser, F., Schiml, S. & Puchta, H. Both CRISPR/Cas-based nucleases and nickases can be used efficiently for genome engineering in *Arabidopsis thaliana*. *Plant J.* **79**, 348–359 (2014).
58. Morineau, C. *et al.* Selective gene dosage by CRISPR-Cas9 genome editing in hexaploid *Camelina sativa*. *Plant Biotechnol. J.* **15**, 729–739 (2017).
59. Bechtold, N. & Pelletier, G. In Planta AgrobacteriumMediated Transformation of Adult Arabidopsis thaliana Plants by Vacuum Infiltration. in *Arabidopsis Protocols* (eds. Martinez-Zapater, J. M. & Salinas, J.) 259–266 (Humana Press, 1998). doi:10.1385/0-89603-391-0:259.
60. Mirdita, M. *et al.* ColabFold - Making protein folding accessible to all. 2021.08.15.456425 Preprint at https://doi.org/10.1101/2021.08.15.456425 (2021).
61. Pettersen, E. F. *et al.* UCSF ChimeraX: Structure visualization for researchers, educators, and developers. *Protein Sci. Publ. Protein Soc.* **30**, 70–82 (2021).
62. Chelysheva, L. A. *et al.* An easy protocol for studying chromatin and recombination protein dynamics during Arabidopsis thaliana meiosis: immunodetection of cohesins, histones and MLH1. *Cytogenet. Genome Res.* **129**, 143–53 (2010).
63. Ross, K. J., Fransz, P. & Jones, G. H. A light microscopic atlas of meiosis in Arabidopsis thaliana. *Chromosome Res* **4**, 507–516 (1996).
64. Vrielynck, N. *et al.* A DNA topoisomerase VI-like complex initiates meiotic recombination. *Science* **351**, 939–943 (2016).
65. Cromer, L. *et al.* Centromeric cohesion is protected twice at meiosis, by SHUGOSHINs at anaphase I and by PATRONUS at interkinesis. *Curr. Biol. CB* **23**, 2090–9 (2013).
66. Lian, Q., Chen, Y., Chang, F., Fu, Y. & Qi, J. inGAP-family: Accurate Detection of Meiotic Recombination Loci and Causal Mutations by Filtering Out Artificial Variants due to Genome Complexities. *Genomics Proteomics Bioinformatics* **20**, 524–535 (2022).
67. Wang, H. *et al.* The cohesin loader SCC2 contains a PHD finger that is required for meiosis in land plants. *PLOS Genet.* **16**, e1008849 (2020).
68. Fernandes, J. B. *et al.* FIGL1 and its novel partner FLIP form a conserved complex that regulates homologous recombination. *PLOS Genet.* **14**, e1007317 (2018).
69. Lu, Y., Ran, J.-H., Guo, D.-M., Yang, Z.-Y. & Wang, X.-Q. Phylogeny and Divergence Times of Gymnosperms Inferred from Single-Copy Nuclear Genes. *PLoS ONE* **9**, e107679 (2014).
70. Bowman, J. L. The liverwort Marchantia polymorpha, a model for all ages. in *Current Topics in Developmental Biology* vol. 147 1–32 (Elsevier, 2022).

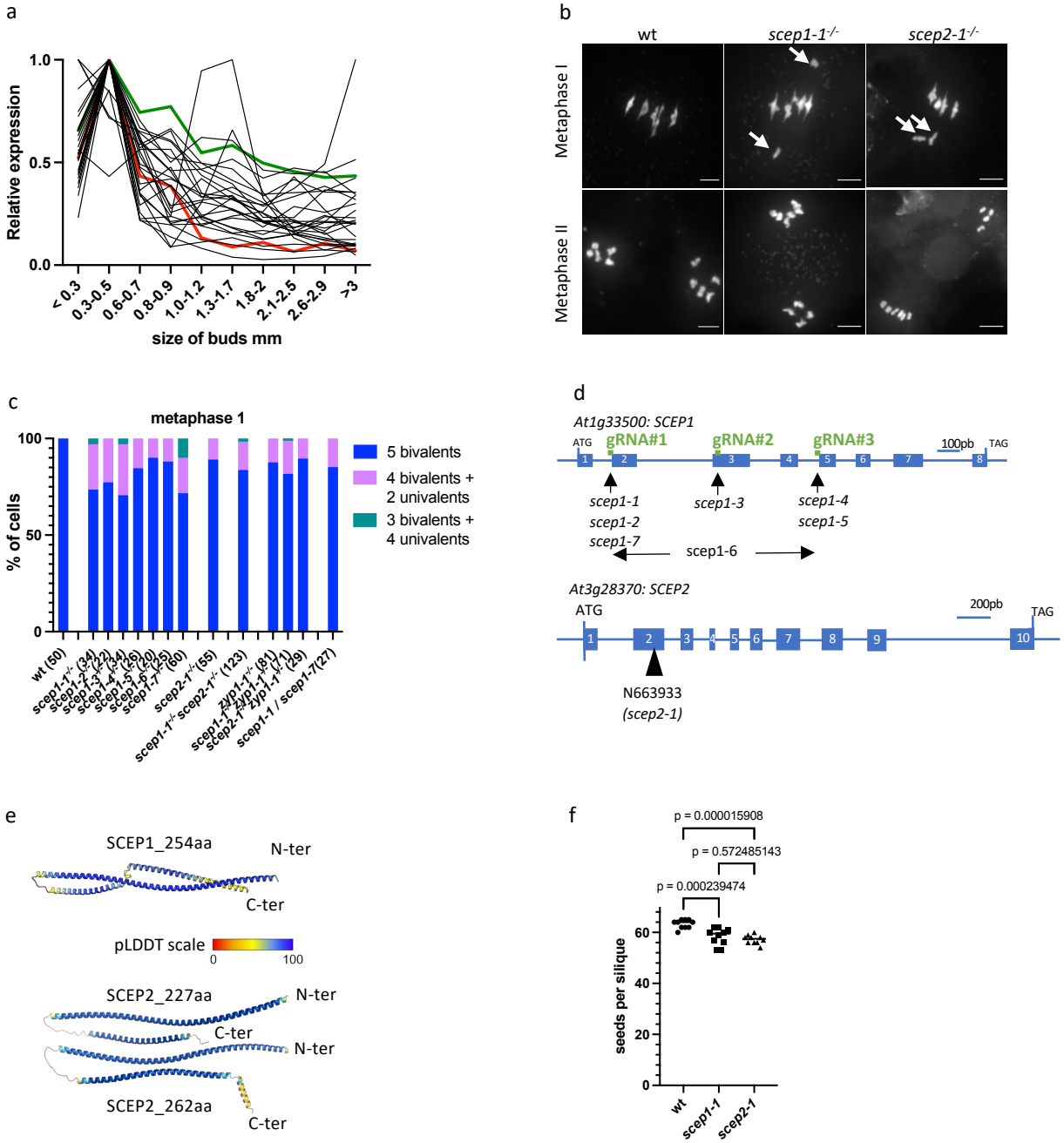

Figure 1. Identification and characterization of SCEP1 and SCEP2

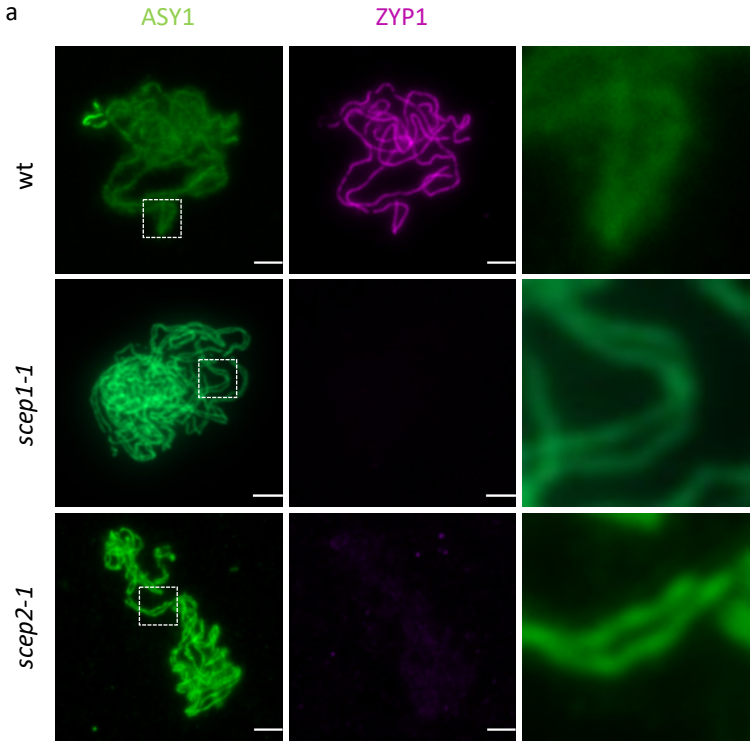

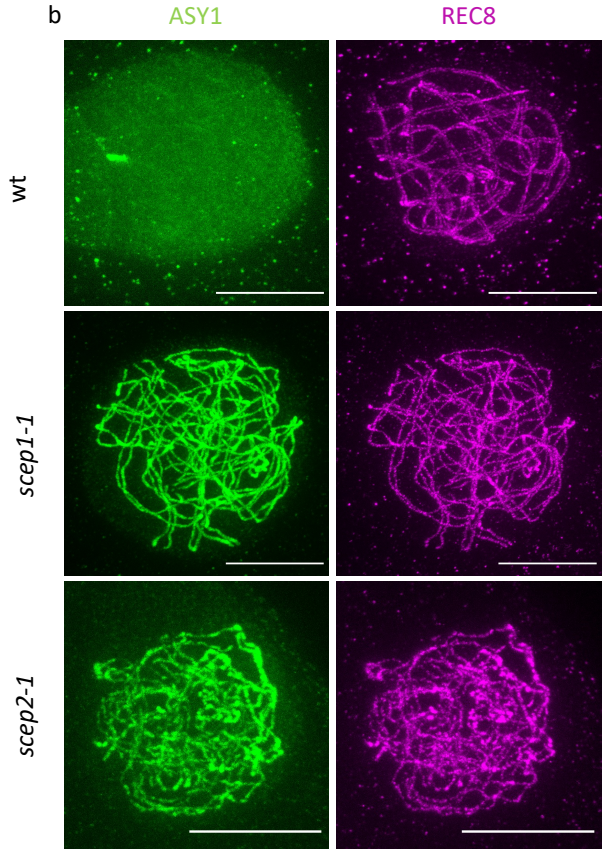

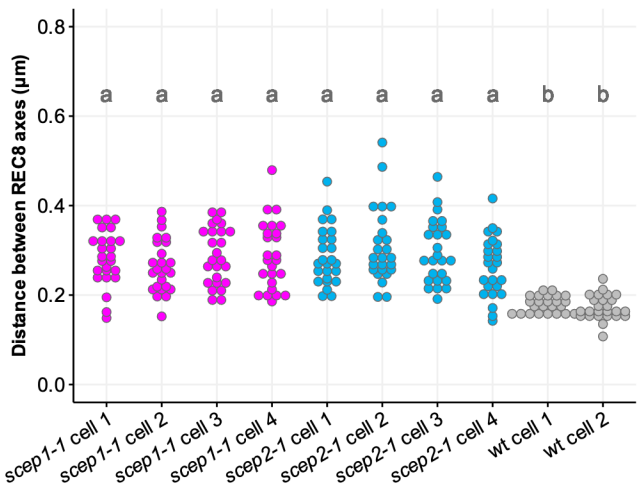

Figure 2. ZYP1s is not loaded in *scep1* and *scep2* mutants

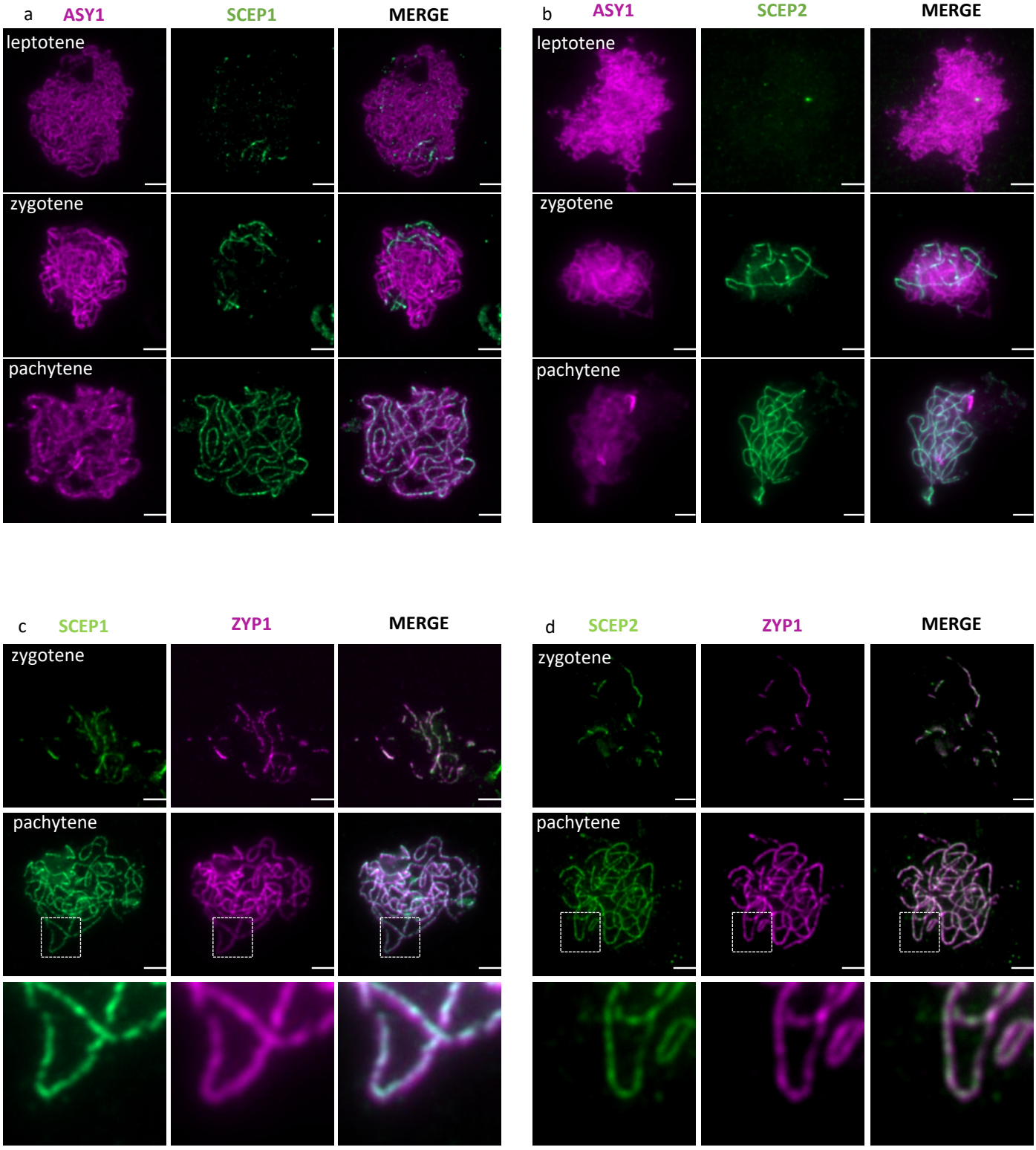

Figure 3. SCEP1 and SCEP2 are loaded on the SC central region

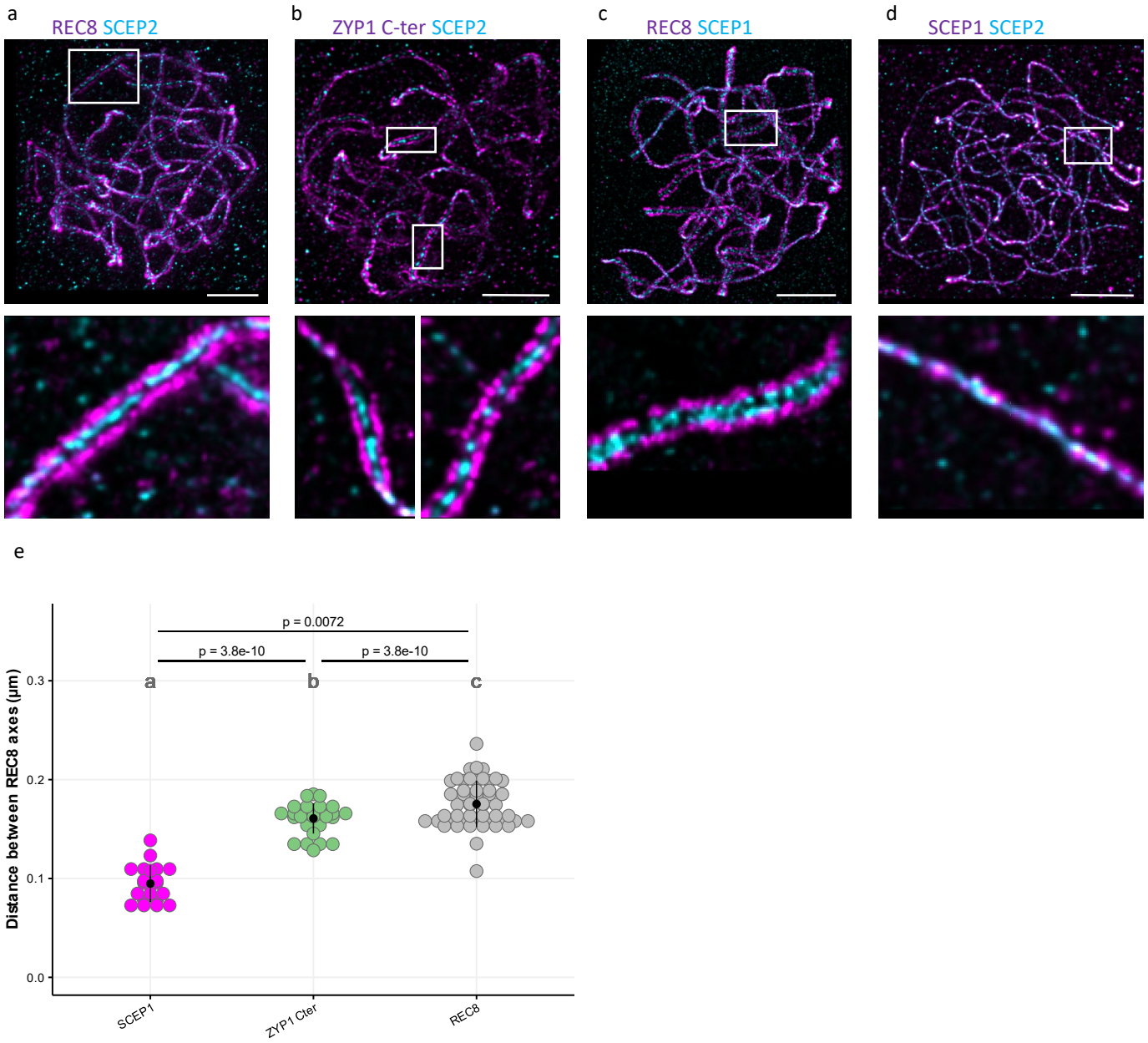

Figure 4. SCEP1 and SCEP2 colocalize at the center of the SC

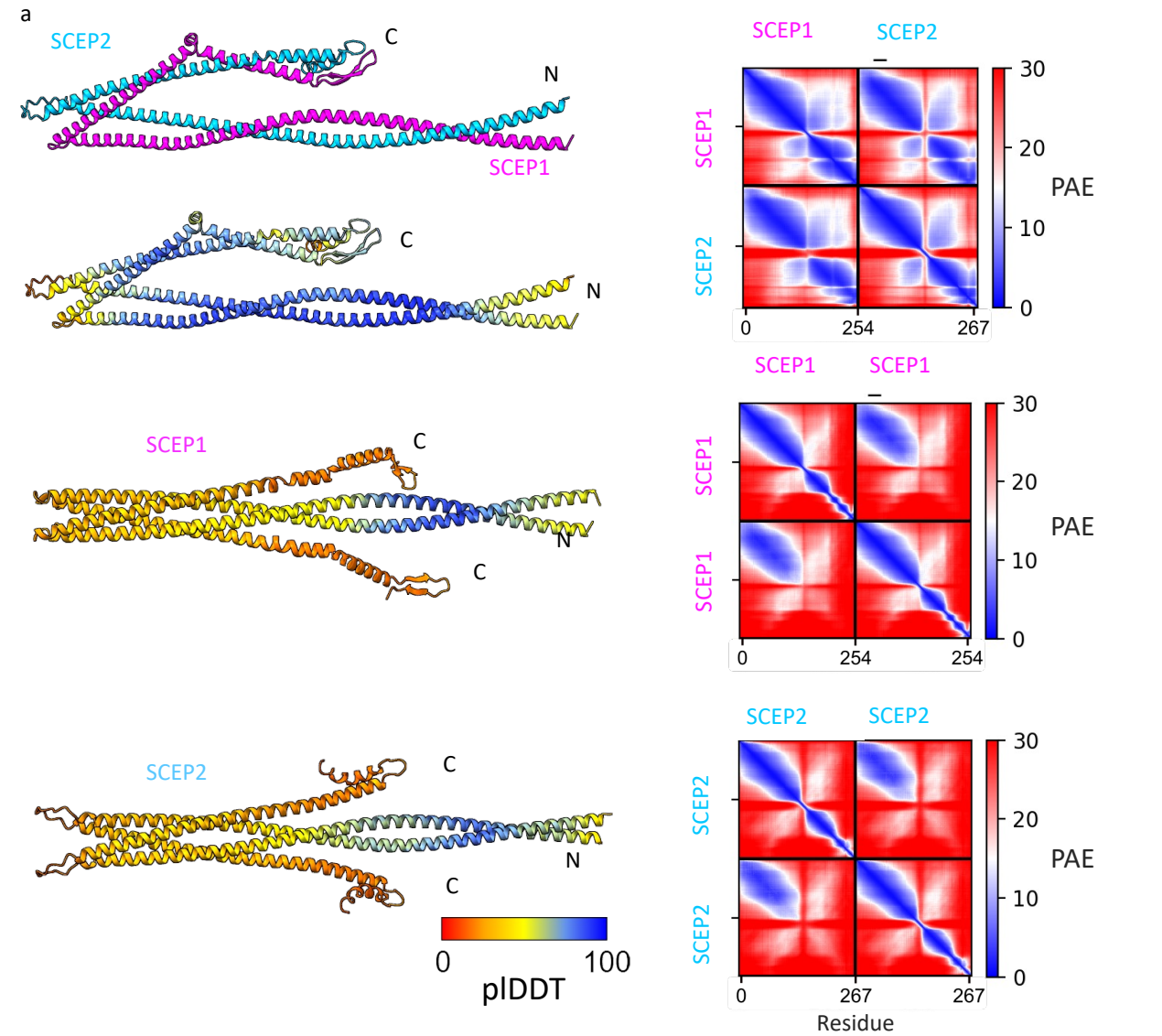

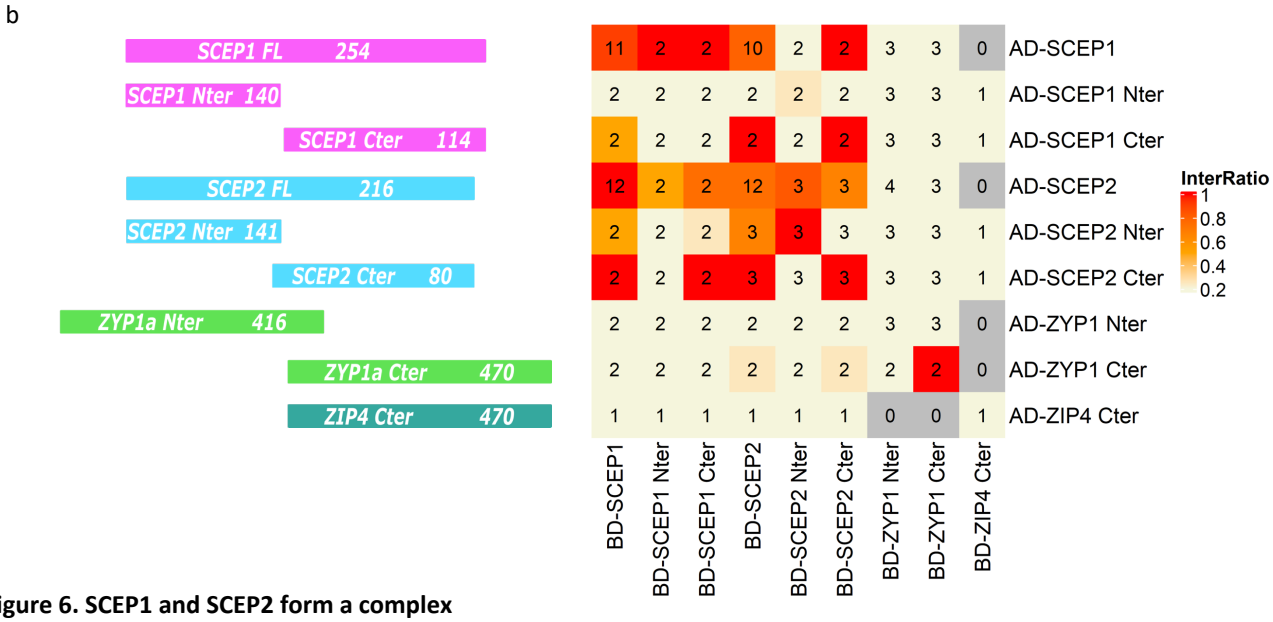

Figure 6. SCEP1 and SCEP2 form a complex

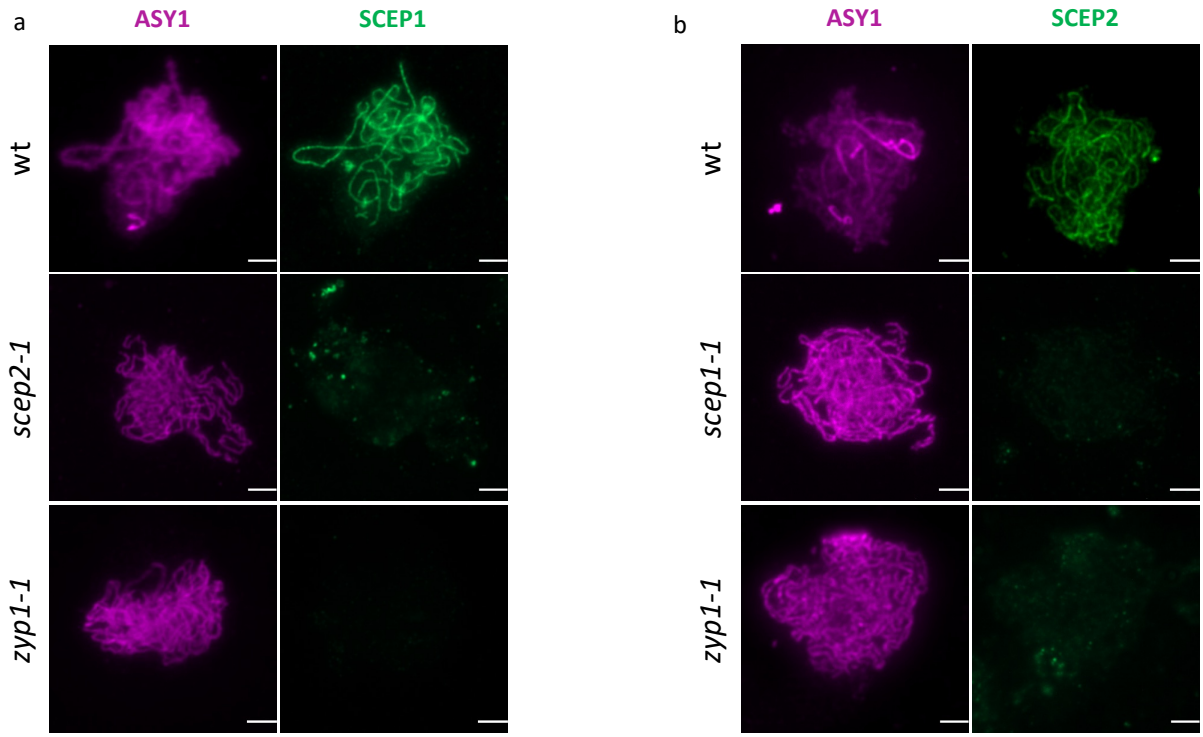

Figure 5. The three proteins SCEP1, SCEP2 and ZYP1 are needed to assemble the SC central region.

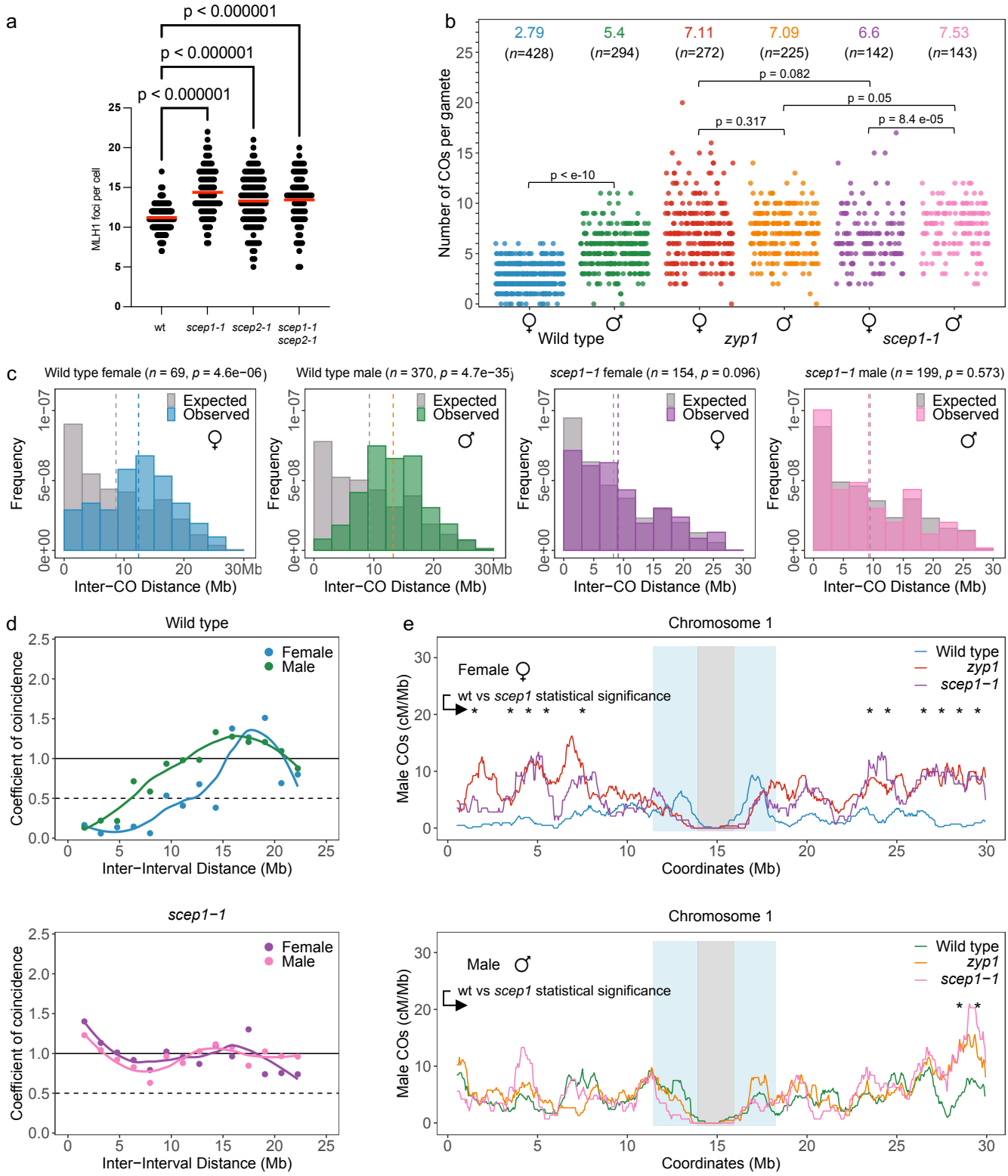

Figure 7: MLH1 foci and COs are increased in CE mutants

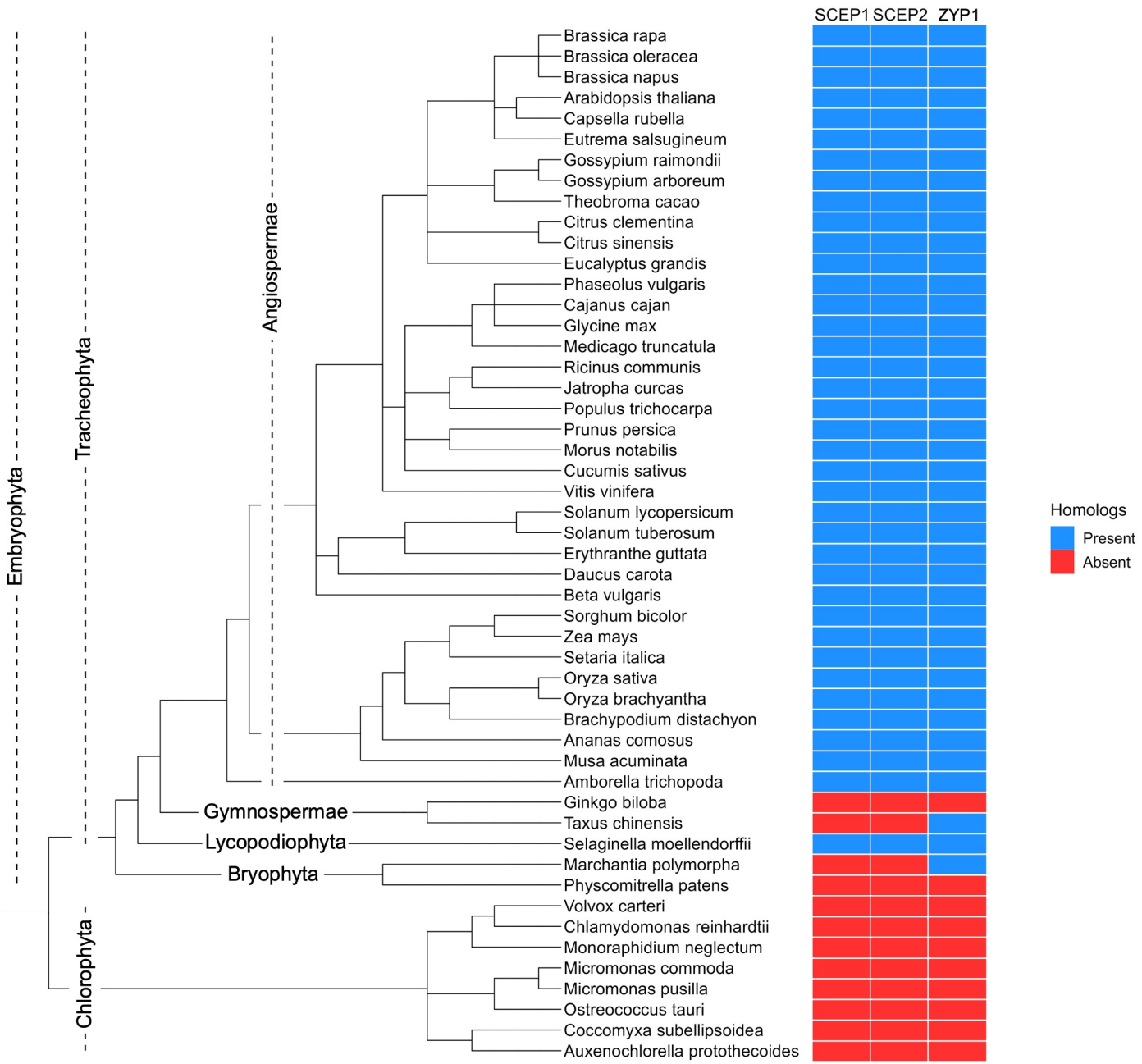

Fig. 8: SCEP1, SCEP2 and ZYP1 homologs can be found in all major angiosperm species.